AD-A087 259 ARCON CORP WALTHAM MA F/G 17/2.1
IONOSPHERIC MODELING AND PROPAGATION ANALYSIS.(U)
APR 80 D C MILLER, J GIBBS F19628-77-C-0051
UNCLASSIFIED RADC-TR-80-29 NL

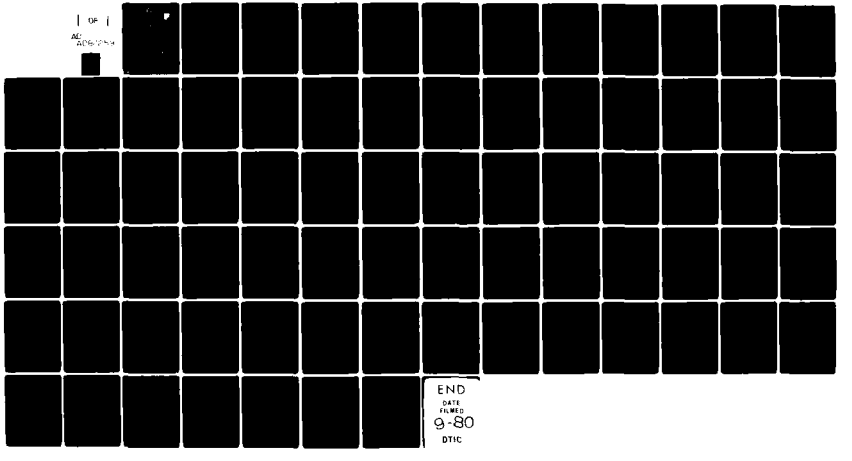

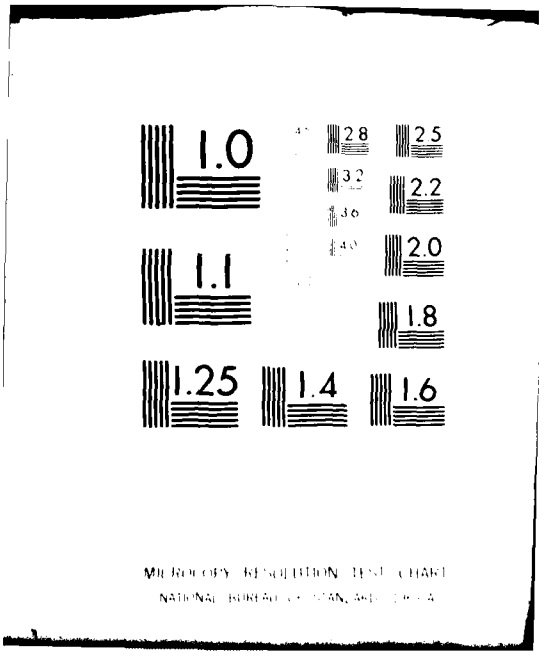
1.0
2.8
2.5
3.2
2.2
3.6
4.0
2.0
1.1
1.8
1.25
1.4
1.6
MICROCOPY RESOLUTION TEST CHART
NATIONAL BUREAU OF STANDARDS-1963-A

LEVEL II

12

AD A062998

RADC-TR-80-29
Final Technical Report
April 1980

IONOSPHERIC MODELING AND PROPAGATION ANALYSIS

Arcon Corporation

David C. Miller
Joseph Gibbs

ROME AIR DEVELOPMENT CENTER
Air Force Systems Command
Griffiss Air Force Base, New York 13441

This report has been reviewed by the RADC Public Affairs Office (PA) and is releasable to the National Technical Information Service (NTIS). At NTIS it will be releasable to the general public, including foreign nations.

RADC-TR-80-39 has been reviewed and is approved for publication.

APPROVED:

GARY S. SALES
Project Engineer

APPROVED:

ALLAN C. SCHELL, Chief
Electromagnetic Sciences Division

FOR THE COMMANDER:

JOHN P. HUSS
Acting Chief, Plans Office

If your address has changed or if you wish to be removed from the RADC mailing list, or if the addressee is no longer employed by your organization, please notify RADC (EEP), Hanscom AFB MA 01731. This will assist us in maintaining a current mailing list.

Do not return this copy. Retain or destroy.

UNCLASSIFIED

SECURITY CLASSIFICATION OF THIS PAGE (When Data Entered)

(19) REPORT DOCUMENTATION PAGE	READ INSTRUCTIONS BEFORE COMPLETING FORM
(18) 1. REPORT NUMBER: RADC-TR-80-29	2. GOVT ACCESSION NO.: AD-A084 259	3. RECIPIENT'S CATALOG NUMBER:
(6) 4. TITLE (and Subtitle): IONOSPHERIC MODELING AND PROPAGATION ANALYSIS	(9) 5. TYPE OF REPORT & PERIOD COVERED: Final Technical Report Nov 76 - Sep 79
	6. PERFORMING ORG. REPORT NUMBER: N/A
(10) 7. AUTHOR(s): David C. Miller, Joseph Gibbs	(15) 8. CONTRACT OR GRANT NUMBER(s): F19628-77-C-0051
9. PERFORMING ORGANIZATION NAME AND ADDRESS: ARCON Corporation, 260 Bear Hill Road, Waltham MA 02154 (16)	10. PROGRAM ELEMENT, PROJECT, TASK AREA & WORK UNIT NUMBERS: 61102F, 2305J220 (17) J1
11. CONTROLLING OFFICE NAME AND ADDRESS: Deputy for Electronic Technology (RADC/EEP), Hanscom AFB MA 01731	12. REPORT DATE: April 1980
	13. NUMBER OF PAGES: 121
14. MONITORING AGENCY NAME & ADDRESS (if different from Controlling Office): Same (11) Apr 80 (12) 75	15. SECURITY CLASS (of this report): UNCLASSIFIED
	15a. DECLASSIFICATION DOWNGRADING SCHEDULE: N/A

16. DISTRIBUTION STATEMENT (of this Report)

Approved for public release; distribution unlimited

17. DISTRIBUTION STATEMENT (of the abstract entered in Block 20, if different from Report)

Same

18. SUPPLEMENTARY NOTES

RADC Project Engineer: Gary S. Sales (RADC/EEP)

19. KEY WORDS (Continue on reverse side if necessary and identify by block number)

Ionospheric Models	Oblique Ionograms
Electron Density Models	Ionospheric Ray Tracing
Ionospheric Parameters	HF Communications Circuits
Vertical Ionograms	Backscatter Ionograms

20. ABSTRACT (Continue on reverse side if necessary and identify by block number)

This report describes several studies and the development of computer techniques toward improving the capability of predicting and assessing HF propagation through the ionosphere. These studies included the development of vertical electron density models which can accurately represent observed oblique and vertical ionograms. These models have been represented by a series of functions which describe the individual ionospheric layers and which are analytically integrable to yield→(over)

DD FORM 1 JAN 73 1473 EDITION OF 1 NOV 65 IS OBSOLETE

UNCLASSIFIED

SECURITY CLASSIFICATION OF THIS PAGE (When Data Entered)

403370 dl

expected ray path trajectories. A computer program has been written which incorporates these features and yields results which are two orders of magnitude faster than those available using conventional numerical ray tracing techniques. The technique has been applied to several studies including the simulation of the backscatter leading edge of oblique ionograms and the determination of HF circuit parameters for a specified ground coverage. The results are presented as a function of the change in individual ionospheric layer parameters.

EVALUATION

This report describes significant advancements in the areas of ionospheric modeling and ray tracing for the purpose of propagation simulation. Techniques are developed for generating electron density profiles from layer parameters and for producing rapid ray traces which will be of appreciable importance to future Air Force requirements

GARY S. SALES
Project Engineer

TABLE OF CONTENTS

Analytic Ray Tracing Techniques and Applications to High Frequency Communication Problems

1. INTRODUCTION

In the development of the computational tools to study radio wave propagation in the ionosphere, it is useful to have exact ray calculations through realistic electron density profiles. The parabolic model ionospheric layer was introduced by Fosterling and Lasser[1] in 1931, and further developed and refined by Appleton and Beynon,[2] and Rawer.[3] This model leads to exact solutions for the vertical ionogram and for horizontally stratified layers, but requires an iterative technique for spherical geometry.

A. H. DeVoogt[4] described the quasi-parabolic layer as an alternative computational tool, which was developed in detail by T. A. Croft and H. Hougasian.[5] This model layer leads to representation of the solutions to the ray equations in terms of the elementary functions.

In addition, D. B. Muldrew[6] introduced a quasi linear election density profile, which was developed in detail by D. E. Westover.[7]

P. A. Bradley and J. R. Dudeney[8] developed a parabolic/linear complete election density profile as a candidate for a standard profile. J. D. Milsom[9] modified the Bradley-Dudeney profile to be represented by Croft and Hougasian type quasi parabolic segments connected by a Westover type quasi linear layer.

All these models are strictly valid for ionospheres which display spherical symmetry. A major problem is to treat in a systematic way the presence of horizontal gradients in the electron density. K. Folkestad[10] described a method of correcting the results of ray calculations through the assumption of tilts in the ionosphere. This technique assumes a spherically symmetric ionosphere, except that the center of curvature is assumed

not necessarily to be at the center of the earth.

The problem of determining the center of curvature of the ionosphere was addressed by R. I. Beckwith,[11] who used the spatial variation of virtual height with parabolic layer theory calculations.

D. Odom (unpublished) used the election density gradient in the neighborhood of the reflection point to construct approximate corrections to the ray trajectories for the effects of horizontal gradients.

No simple technique appears to be forthcoming to handle the effects of the geomagnetic field or neutral collisions; however, ionospheric absorption may be calculated for field strength calculations by using a semi-empirical model such as the Bradley-George[12] absorption model.

The next section is devoted to a development of the ray equations from the Hamiltonian equations described by J. Haselgrove;[13] the approach is, firstly, ignoring the magnetic field and collisions, and, secondly, from an assumption of nearly spherically symmetric ionosphere. Equations are developed which allow an approximate correction for the effects of horizontal gradients, which may be applied after calculation of the major ray parameters through a given layer.

Section 3 describes the quasi-parabolic ray calculation equations, and the options available for segmenting profiles with quasi-parabolic, inverted quasi parabolic, and quasi-linear layers.

Section 4 describes the Bradley-Dudeney profile and suggested modifications to quasi parabolic/quasi linear models, and Section 5 describes the piecewise smooth quasi parabolic profile with various construction options.

In Section 6 we discuss models for simulation of ionospheric parameters, updating techniques based on real time ionograms, and profile modifications to account for horizontal gradients. Section 7 is devoted to applications of the model to transmission circuits, while Section 8 describes applications to vertical and oblique ionogram simulation.

Section 9 is devoted to program descriptions and listings and may serve as a user guide to the program modules implementing the ray calculations.

2. DEVELOPMENT OF THE RAY EQUATIONS

When the effects of the earth's magnetic field and electron collisions may be neglected, the equations [12] governing electromagnetic wave trajectories are given by,

$$\dot{r} = V_r \tag{2.1}$$

$$\dot{\theta} = V_\theta / r \tag{2.2}$$

$$\dot{\varphi} = V_\varphi / r \sin\theta \tag{2.3}$$

$$\dot{V}_r = \mu \frac{\partial \mu}{\partial r} + V_\theta \dot{\theta} + V_\varphi \sin\theta \dot{\varphi} \tag{2.4}$$

$$r\dot{V}_\theta = \mu \frac{\partial \mu}{\partial \theta} - V_\theta \dot{r} + r V_\varphi \cos\theta \dot{\varphi} \tag{2.5}$$

$$r \sin\theta \dot{V}_\varphi = \mu \frac{\partial \mu}{\partial \varphi} - V_\varphi \sin\theta \, \dot{r} - r V_\varphi \cos\theta \, \dot{\theta} \tag{2.6}$$

where r, θ, φ are the spherical polar coordinates of a point on the ray path, V_r, V_θ, V_φ are the components of the ray normal direction in the r, θ, and φ directions so normalized that

$$V_r^2 + V_\theta^2 + V_\varphi^2 = \mu \tag{2.7}$$

The phase refractive index μ, in the no field, no collision case is given by

$$\mu^2 = 1 - (f_p/f)^2 \tag{2.8}$$

where f_p is the local plasma frequency and f is the radiation frequency; in in this case, the group refractive index $\mu' = \frac{d}{df}(f\mu)$ is given by

$$\mu' = 1/\mu \tag{2.9}$$

The independent variable t is the group path defined by (no field, no collision)

$$t = \int \mu' \, ds \tag{2.10}$$

Equation (2.6) may be immediately rewritten as

$$\frac{d}{dt}(r \sin\theta \, V_\varphi) = \frac{1}{2} \frac{\partial \mu^2}{\partial \varphi} \tag{2.11}$$

and equations (2.5) and (2.6) may be combined as

$$\frac{d}{dt}(rV_H)^2 = r^2 \dot{\theta}\left[\frac{\partial \mu}{\partial \theta}^2 + \frac{d\varphi}{d\theta}\frac{\partial \mu}{\partial \varphi}^2\right] \tag{2.12}$$

where $V_H = \sqrt{V_\theta^2 + V_\varphi^2} = \mu \cos\beta$

and β is the local elevation angle.

In the absence of horizontal gradients in the refractive index, Equation (2.11) expresses the requirement of great circle propagation, and Equation (2.12) is the well known Bouger's rule, $\mu r \cos\beta$ is a constant of the motion. Furthermore, the ray trajectory equations can be reduced to quadratures in the radial coordinate,

$$\Theta(r) = (\mu_o \, r_o \cos\beta_o) \int_{r_o}^{r} \frac{dr'}{r' Z(r')} \tag{2.13}$$

$$P'(r) = \int_{r_o}^{r} \frac{r' \, dr'}{Z(r')} \tag{2.14}$$

$$P(r) = \int_{r_o}^{r} \frac{r' \, \mu^2(r') \, dr'}{Z(r')} \tag{2.15}$$

$$Z(r) = \mu(r) \, r \sin\beta(r) = \left[(\mu r)^2 - (\mu_o \, r_o \cos\beta_o)^2\right]^{1/2} \tag{2.16}$$

where $\Theta(r)$, $P'(r)$, and $P(r)$ are respectively the ground range (in radians), the group path length, and the phase path length accrued along the ray trajectory between entering a layer at r_o and the point on the trajectory at height r. Integration extends to ray apogee or perigee ($Z = 0$) or to

penetration through the layer, whichever is appropriate.

If the horizontal gradients in the index of refraction are small enough, the Equations (2.13) through (2.15), suitably implemented, remain good approximations to the ray path parameters. The effects of horizontal components of gradients, then, may be estimated and applied as corrections to the local elevation angle and deviation to great circle propagation. From Equation (2.8), partial derivitives of the phase refractive index may be written as

$$\frac{\partial \mu}{\partial \chi} = 2(\mu^2 - 1)\frac{\partial}{\partial \chi} (\log f_p) \tag{2.17}$$

Consider first the case where the component transverse to the plane of ray propagation vanishes, and let θ be the ground range and φ the relative bearing from that plane. Great Circle propagation still pertains, thus, $V_\varphi(t) = 0$, $\varphi(t) = 0$, $V_H(t) = r\dot{\theta}$, and from Equation (2.12),

$$\frac{d}{dt}(\mu r \cos\beta) = \frac{\partial}{\partial \theta}(\log f_p)(\mu^2 - 1) \tag{2.18}$$

If the longitudinal gradient of $\log f_p$ can be considered sufficiently constant, then the above may be integrated to give the change in the Bouger invariant due to this gradient accrued through the layer.

$$\Delta(\mu r \cos\beta) = (P - P') \frac{\partial}{\partial \theta} (\log f_p) \tag{2.19}$$

This correction, then, should be fed back into the integrals, Equations (2.13) through (2.15), for recalculation. This process may be reiterated, if desired, until stability of the computation is achieved.

In the presence of transverse gradients Equation (2.11) can be similarly integrated to provide the accrual to the invariant $r \sin\theta V_\varphi$, thus,

$$\Delta(r \sin\theta\, V_\varphi) = (P - P') \frac{\partial}{\partial \varphi} (\log f_p) \tag{2.20}$$

or

$$r \sin\theta V_\varphi = r_\circ \sin\theta_\circ V_{\varphi\circ} + (P - P')\frac{\partial}{\partial\varphi}(\log f_p)$$

from which,

$$\frac{d\varphi}{d\theta} = \left[\frac{r \sin\theta V_\varphi}{\mu r \cos\beta}\right] 1/\sin^2\theta \qquad (2.21)$$

and

$$\varphi(\theta) = \varphi_\circ + A \sin(\theta_\circ - \theta) \qquad (2.22)$$

where

$$A = \left[\frac{r \sin\theta V_\varphi}{\mu r \cos\beta}\right]_{AVG} \circ \frac{1}{\sin\theta \sin\theta_\circ} \qquad (2.23)$$

Finally the contribution from the transverse gradient can be included in Equation (2.19), thus

$$\Delta(\mu r \cos\beta) = (P - P')\left\{\frac{\partial}{\partial\theta}\log f_p + A \frac{\partial}{\partial\varphi}\log f_p\right\} \qquad (2.24)$$

Clearly, any implementation of these last few equations in numerical calculations must be careful to avoid the kinematic singularity at $\theta = 0$. The best technique would be to arrange the calculation so that the reflection point occurs approximately $\pi/2$ from the pole of the coordinate system.

3. INTEGRATION OF THE RAY EQUATIONS THROUGH QUASI-PARABOLIC LAYERS

The parabolic model of election density has been for many years very popular as a technique to simulate and study the phenomenom of ionospheric radio propagation. This model expresses the electron density kf_p^2 by the equation of a parabola, to wit,

$$f_p^2(r) = f_c^2 \left[1 - \left(\frac{r - r_m}{y_m}\right)^2\right] \quad r_m - y_m < r < r_m + y_m \qquad (3.1)$$
$$= 0 \qquad \text{elsewhere}$$

where $f_p(r)$ is the plasma frequency having a maximum value of f_c at the layer semi-thickness, and r is the radial distance from the center of the earth.

For vertical incidence ($\mu r \cos \beta = 0$) this model allows solutions for Θ, P', and P in terms of elementary functions, for in this case

$$Z(r) = r\,\mu(r)$$

and the integrals for P' and P ($\Theta = 0$ trivially) take the form

$$P'(r) = \int \frac{dr}{\sqrt{a\,r^2 + b\,r + c}} \qquad (3.2)$$
$$P(r) = \int \sqrt{a\,r^2 + b\,r + c}\; dr$$

However, for oblique propagation the expression under the radical is a quartic, and Θ, P', and P are represented by elliptic integrals which do not allow for representation in terms of the elementary functions. On the other hand, the virtual height method has been developed to approximate the solution for P' on the oblique path from the vertical solution for the equivalent vertical frequency.

As pointed out by several investigators (References 4, 5, 6, 7, 9) a minor modification to the parabolic model permits the representation of

the ray-path parameters in terms of elementary functions. This modification is known as the Quasi-Parabolic (QP) Model layer and given by

$$f_p^2(r) = f_c^2 \left[1 - \left(\frac{r - r_m}{y_m} \cdot \frac{r_b}{r}\right)^2\right] \quad r_b < r < r_b' \qquad (3.3)$$

$$= 0 \qquad \text{elsewhere}$$

where $r_b = r_m - y_m$

and $r_b' = r_m + y_m \left[r_m \Big/ \left(r_m - 2y_m\right)\right]$

For typical values of r_m and y_m (6800 and 100 respectively) the additional term r_b/r would cause a difference of a few percent at most from the parabolic layer, and primarily in the topside of the layer.

The advantage of the QP model is clearly seen if we note that

$$Z^2(r) = (\mu r)^2 - (\mu_o r_o \cos \beta_o)^2 = r_m^2 \left(Ax^2 - 2Bx + C\right) \qquad (3.4)$$

where

$$x = r/r_m$$

$$A = 1 - X_C + X_G$$

$$B = X_G$$

$$C = X_G - \Gamma$$

$$X_C = (f_c/f)^2$$

$$X_G = X_C (r_m/y_m - 1)^2$$

$$\Gamma = (\mu_o r_o \cos \beta_o / r_m)^2$$

The equations for ground range, group path and phase path, then, have solutions in terms of elementary functions as follows

$$\Theta(r) = \Gamma F_2$$

$$P'(r) = r_m \left[F_1 + B F_3\right] / A$$

$$P(r) = r_m \left[F_1 - B F_3 + (C + \Gamma) F_2\right] \qquad (3.5)$$

where $F_1 = Y(x) - Y(x_o)$

$$F_2 = \int_{x_o}^{x} dx'/x' \, Y(x')$$

$$F_3 = \int_{x_o}^{x} dx'/Y(x')$$

$$Y(x) = (Ax^2 - 2Bx + C)^{1/2} \qquad (3.6)$$

These may be integrated to yield

$$F_2 = \frac{1}{\gamma} \text{LOG} \left\{ \frac{x(Bx_o - C - \gamma Y_o)}{x_o(Bx - C - \gamma Y)} \right\} \qquad C>0$$

$$= (x_o Y - x Y_o)/(Bx x_o) \qquad C=0,\ B\neq 0$$

$$= (x - x_o)/\alpha x x_o \qquad C=0,\ B=0$$

$$= \frac{1}{\gamma} \text{ATAN} \left\{ \frac{\gamma Y(Bx_o - C) - \gamma Y_o(Bx - C)}{(Bx_o - C)(Bx - C) - C Y_o Y} \right\} \qquad C<0 \qquad (3.7)$$

$$F_3 = \frac{1}{\alpha} \text{LOG} \left\{ \frac{B - Ax - \alpha Y}{B - Ax_o - \alpha Y_o} \right\} \qquad A>0$$

$$= (Y_o - Y)/B \qquad A=0,\ B\neq 0$$

$$= (x - x_o)/\gamma \qquad A=0,\ B=0$$

$$= \frac{1}{\alpha} \text{ATAN} \left\{ \frac{\alpha Y_o (B - Ax) - \alpha Y (B - Ax_o)}{(B - Ax)(B - Ax_o) - A Y Y_o} \right\} \qquad A<0 \qquad (3.8)$$

where $x = r/r_m$, $x_o = r_o/r_m$, $Y = Y(x)$, $Y_o = Y(x_o)$

and $\alpha^2 = |A|$, $\gamma^2 = |C|$.

The ray is assumed to enter the ionospheric layer at r_o, and the upper limit r is the other boundary of the layer, unless reflection occurs. This condition occurs when Z vanishes ($Z = \mu r \sin\beta$)

or $$Ax_r^2 - 2B x_r + C = 0 \qquad (3.9)$$

If both solutions to this quadratic equation are physically valid, then one solution belongs to the ray entering from below and reflecting downwards, while the other belongs to the ray entering from above and reflecting upwards. After reflection the ray would be carried back to the appropriate boundary by doubling the accumulated group path, phase path and range.

When a QP layer is employed as a model for the E or F ionospheric layers ($y_m << r_m$, $F_p \leq F_c$) A is always positive while C remains positive up to the UHF band, thus the LOG forms prevail for functions F_2 and F_3. On the other hand one may desire to turn the parabola over for use as bottomside or topside tails, or as a fitting layer between two layers with local maxima. This inverted QP layer is given by

$$X(r) = (F_p/f)^2 = X_L + X_A (r_m/r - 1)^2 \qquad (3.10)$$

with $X_L \geq 0 \quad X_A > 0.$

In this case,

$$A = 1 - X_L - X_A$$

$$B = - X_A$$

$$C = - X_A - \Gamma \qquad (3.11)$$

Clearly C is always negative while A is negative except at high frequencies; thus the ATAN forms prevail for functions F_2 and F_3.

Another model layer with this same class of solutions is the quasi-linear layer given by

$$X(r) = X_m \pm 2 X_L (1 - r_m/r) \qquad (3.12)$$

in which case

$$A = (1 - X_m \mp 2 X_L)$$
$$B = \pm 2 X_L$$
$$C = -\Gamma$$

Clearly C is negative, thus the ATAN form applies for function F_2 while A may be positive or negative. Note that the quasi-linear layer defined by Equation (3.12) is not the same as that treated by Westover [7] and by Milsom.[9]

These three functional forms, the quasi-parabolic, the inverted quasi-parabolic, and the quasi-linear, form a stable of candidates for segments of ionospheric layers which allow the construction of election density profiles with substantial variation; one may construct, segment by segment, peaks and valleys and tails. For any such profile the contributions to ground range, group path, and phase path may be calculated in each segment, from essentially the same class of solutions, and then summed for the entire ray trajectory.

4. THE MODIFIED BRADLEY DUDENEY PROFILE

P. A. Bradley and J. R. Dudeney[8] described an idealized model for election density profiles generated from four ionospheric parameters, f_oE, f_oF_2, h_mF_2 and y_mF_2 (see Table I for definitions of ionospheric parameter notation). This model consists of parabolic E and F layers connected by a linear increase in electron density between h_mE and a point on the F_2 parabolic layer where the plasma frequency is equal to $1.7\ f_oE$. This model is described in detail in Table II.

Milsom[9] showed how this model may be modified slightly using quasi parabolic E and F layers connected by a "quasi linear" layer of the form

$$N(r) = N_m(r^2 - r_b^2)/(r_m^2 - r_b^2) \qquad (4.1)$$

which had previously been shown by D. B. Muldrew[6] and D. E. Westover[7] to allow analytic integration of the ray equations in terms of elementary functions.

Note that the Muldrew/Westover/Milsom quasi linear form differs from that introduced in the last section, Equation (3.12), and that the integration of the ray equations will differ as a consequence. It is suggested that the functional form of Equation (3.12) is also a suitable candidate for the intermediate layer, with the advantage that solutions to the ray equations are selected from a single subset of functions.

In order to compare the three candidates, the Milsom layer, Equation (4.1) may be written as

$$N(r) = N_E + N_Y\left[r_E/(r_E + r_j)\right]\left[(r/r_E)^2 - 1\right] \qquad (4.2)$$

Applying the condition $N(r_j) = N_j$, then

$$N_Y = (N_j - N_E)\, r_E/(r_j - r_E) \tag{4.3}$$

which is the same expression for the equivalent term in the Bradley Dudeney intermediate layer.

On the other hand if one uses Equation (3.12) as the intermediate layer one may write,

$$N(r) = N_j + N_Y\,(1 - r_E/r) \tag{4.4}$$

in which case N_Y is given by,

$$N_Y = (N_j - N_E) \cdot r_j/(r_j - r_E) \cdot \tag{4.5}$$

No substantial difference obtains between intermediate layers (4.2) and (4.4); we do present the specifications based upon intermediate layer (4.4) in Table III; the graph of this profile is shown in Figure 4.1.

TABLE I.

Definitions of Ionospheric Terms

r_o	-	radius of earth
$f_o E$	-	E layer critical frequency
$h_m E$	-	E layer height
$y_m E$	-	E layer semi-thickness
$f_o F_1$	-	F_1 layer critical frequency
$h_m F_1$	-	F_1 layer height
$y_m F_1$	-	F_1 layer semi-thickness
$f_o F_2$	-	F_2 layer critical frequency
$h_m F_2$	-	F_2 layer height
$y_m F_2$	-	F_2 layer semi-thickness
$N(r)$	-	Electron Density Profile
$f_p(r)$	-	Plasma Frequency Profile
k	-	$N(r)/f_p(r) = 1.24E4\ (\text{mhz})^{-2}\ (\text{cm})^{-3}$

TABLE II

Specifications for Bradley-Dudeney Profile

$$N(r) = 0 \qquad r \leq r_b$$

$$N(r) = N_E - N_X (r/r_E - 1)^2 \qquad r_b \leq r \leq r_E$$

$$N(r) = N_E + N_Y (r/r_E - 1) \qquad r_E \leq r \leq r_j$$

$$N(r) = N_F - N_Z (r/r_F - 1)^2 \qquad r_j \leq r \leq r_t$$

$$N(r) = 0 \qquad r_t \leq r$$

$$r_b = r_E - y_m E$$

$$r_E = r_o + h_m E$$

$$r_j = r_F - y_m F_2 (1 - N_j/N_F)^{1/2}$$

$$r_F = r_o + h_m F_2$$

$$r_t = r_F + y_m F_2$$

$$r_{bF} = r_F - y_m F_2$$

$$N_E = k (f_o E)2$$

$$N_F = k (f_o F_2)^2$$

$$N_j = k (1.7 f_o E)^2$$

$$N_X = N_E (r_E/y_m E)^2$$

$$N_Z = N_F (r_F/y_m F)^2$$

$$N_Y = (N_j - N_E) \cdot r_E/(r_j - r_E)$$

TABLE III

Specifications for the Modified Bradley-Dudeney Profile (MBD)

$$N(r) = 0 \qquad r \le r_b$$

$$N(r) = N_E - N_X(1 - r_E/r)^2 \qquad r_b \le r \le r_E$$

$$N(r) = N_E + N_Y(1 - r_E/r) \qquad r_E \le r \le r_j$$

$$N(r) = N_F - N_Z(1 - r_F/r)^2 \qquad r_j \le r \le r_t$$

$$N(r) = 0 \qquad r_t \le r$$

$$r_b = r_E - y_m E$$

$$r_E = r_o + h_m E$$

$$r_j = r_F\, r_{bF} / \left\{ r_{bF} + y_m F_2 \left(1 - N_j/N_F\right)^{1/2} \right\}$$

$$r_F = r_o + h_m F_2$$

$$r_t = r_F\, r_{bF} / (r_{bF} - y_m F_2)$$

$$r_{bF} = r_F - y_m F_2$$

$$N_E = k\,(f_o E)^2$$

$$N_F = k\,(f_o F_2)^2$$

$$N_j = k\,(1.7\, f_o E)^2$$

$$N_X = N_E (r_b / y_m E)^2$$

$$N_Z = N_F (r_{bF} / y_m F_2)^2$$

$$N_Y = (N_j - N_E)\, r_j / (r_j - r_E)$$

Modified Bradley-Dudeney Electron Density Profile

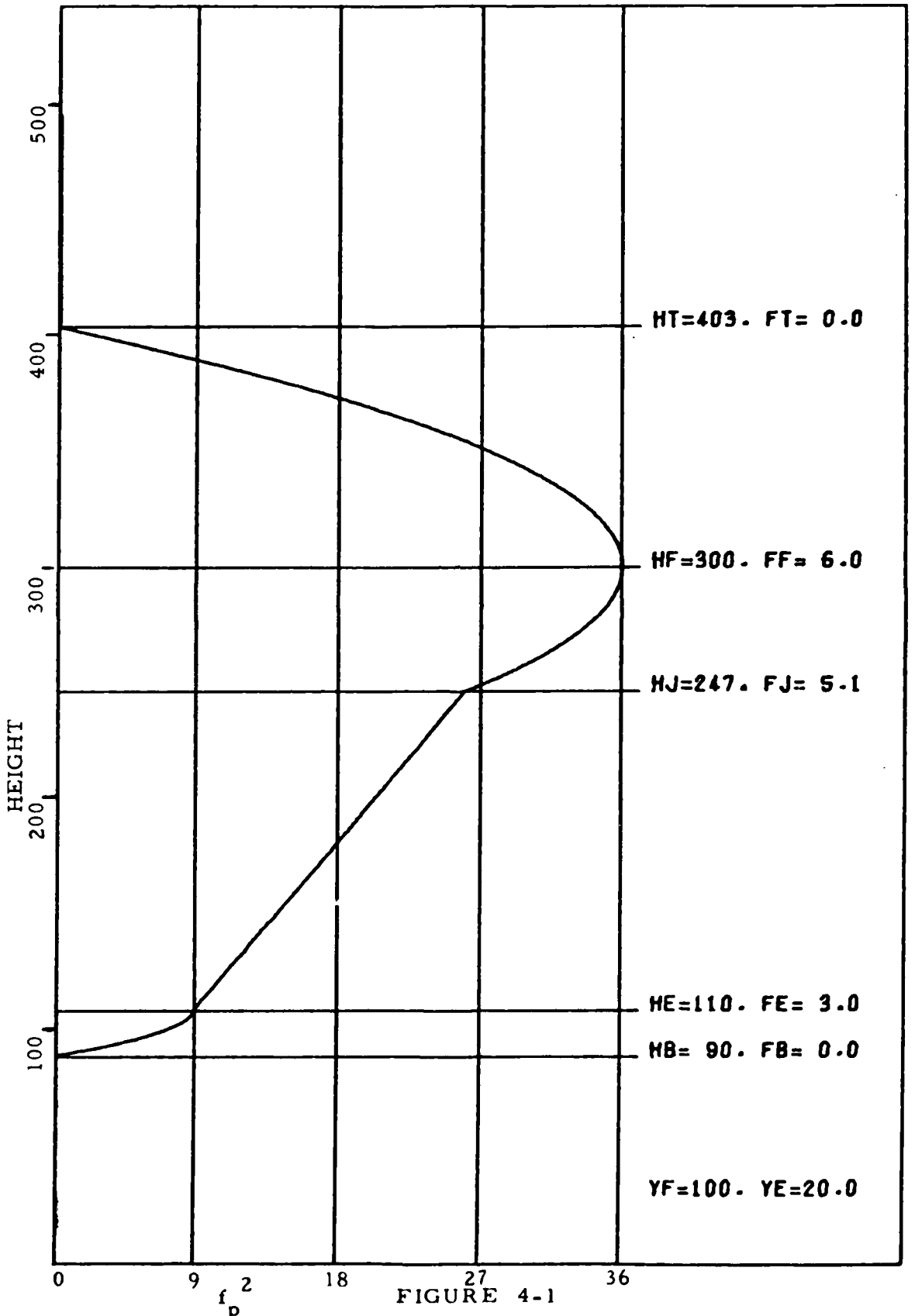

FIGURE 4-1

5. PIECEWISE SMOOTH QUASI PARABOLIC PROFILES

A Piecewise Smooth Quasi Parabolic Profile (PSQP) consists of alternating quasi-parabolic segments fitted together in such a manner that the electron density and its first derivative is continuous at each fitting point. Consider two such segments with a QP segmented fitted below an inverted QP segment

$$\begin{aligned} N(r) &= N_E - N_B (1 - r_E/r)^2 \qquad r_b \le r \le r_x \\ N(r) &= N_C + N_D (1 - r_C/r)^2 \qquad r_x \le r \le r_y \end{aligned} \tag{5.1}$$

Continuity of the electron density and its derivative at the fitting point r_x demands that

$$\begin{aligned} N_C + N_D (1 - r_c/r_x)^2 &= N_E - N_B (1 - r_E/r_X)^2 \\ r_C N_D (r_c - r_x) &= r_E N_B (r_x - r_E) \end{aligned} \tag{5.2}$$

or equivalently,

$$\begin{aligned} N_D &= N_B \; r_E (r_x - r_E)/r_c (r_c - r_x) \\ N_B (r_x - r_E) (r_c - r_E) &= (N_E - N_c) r_c r_x \end{aligned} \tag{5.3}$$

If the QP segment is specified ad hoc (N_E, N_B, r_E are given), then we have two conditions to determine four parameters (N_C, N_D, r_c, and r_x); thus two parameters may be determined by two independant arbitrary conditions. For example, a topside (or bottomside) tail may be constructed which goes smoothly to zero ($N_c = 0$), at a specified point (r_c is given), or fitted at a specified point (r_x is given); or a valley may be constructed ($N_C < N_A$ is given) at r_c or fitted at r_x. The algebra to solve for the

the remaining parameters is straight forward.

Between two QP segments a valley can be constructed from an inverted QP segment fitted smoothly to both QP segments. In this case we have four continuity conditions for five parameters (N_C, N_D, r_c, r_x, r_y) if the top QP layer is given

$$N(r) = N_F - N_G(1 - r_F/r)^2 \qquad r_y \le r \le r_F \tag{5.4}$$

To determine the intermediate layer, one may arbitrarily choose the valley depth $\Delta N \ge 0$ such that $N_C = N_E - \Delta N$ and the remaining parameters are determined from the four continuity conditions. Again the algebra is straight forward. Electron density profiles with $\Delta N = 0$, $1/2\, f_o E$, and $f_o E$ are shown in Figures 5.1, 5.2 and 5.3.

Another interesting criterior to impose on the intermediate layer is the scale independent condition, expressed by

$$\begin{aligned} N_E r_x r_y &= N_B (r_x - r_E)(r_y - r_E) \\ N_F r_x r_y &= N_G (r_F - r_x)(r_F - r_y) \end{aligned} \tag{5.5}$$

Note that each of these two conditions are independent of a scale change of either QP layer; the solutions for the fitting points and r_y depend only upon the layer heights and semi thicknesses of the two QP layers. Thus, in an electron density model where only $f_o E$ and $f_o F_2$ vary, the fitting points do not change. The algebra is straight forward to demonstrate that these conditions satisfy the continuity conditions.

The parameters r_x and r_y are, then, given by the solutions to the quadratic equation $A r^2 - B r + C = D$, where

$$A = r_F N_G (N_B - N_E) - r_E N_B (N_E - N_F)$$

$$B = r_F^2 N_G (N_B - N_E) - r_E^2 N_B (N_E - N_F) \qquad (5.6)$$

$$C = r_E r_F (r_F - r_E) N_B N_G$$

An electron density profile satisfying conditions (5.5) is shown in Figure 5.4.

PSQP Electron Density Profile, $F_L = F_E$

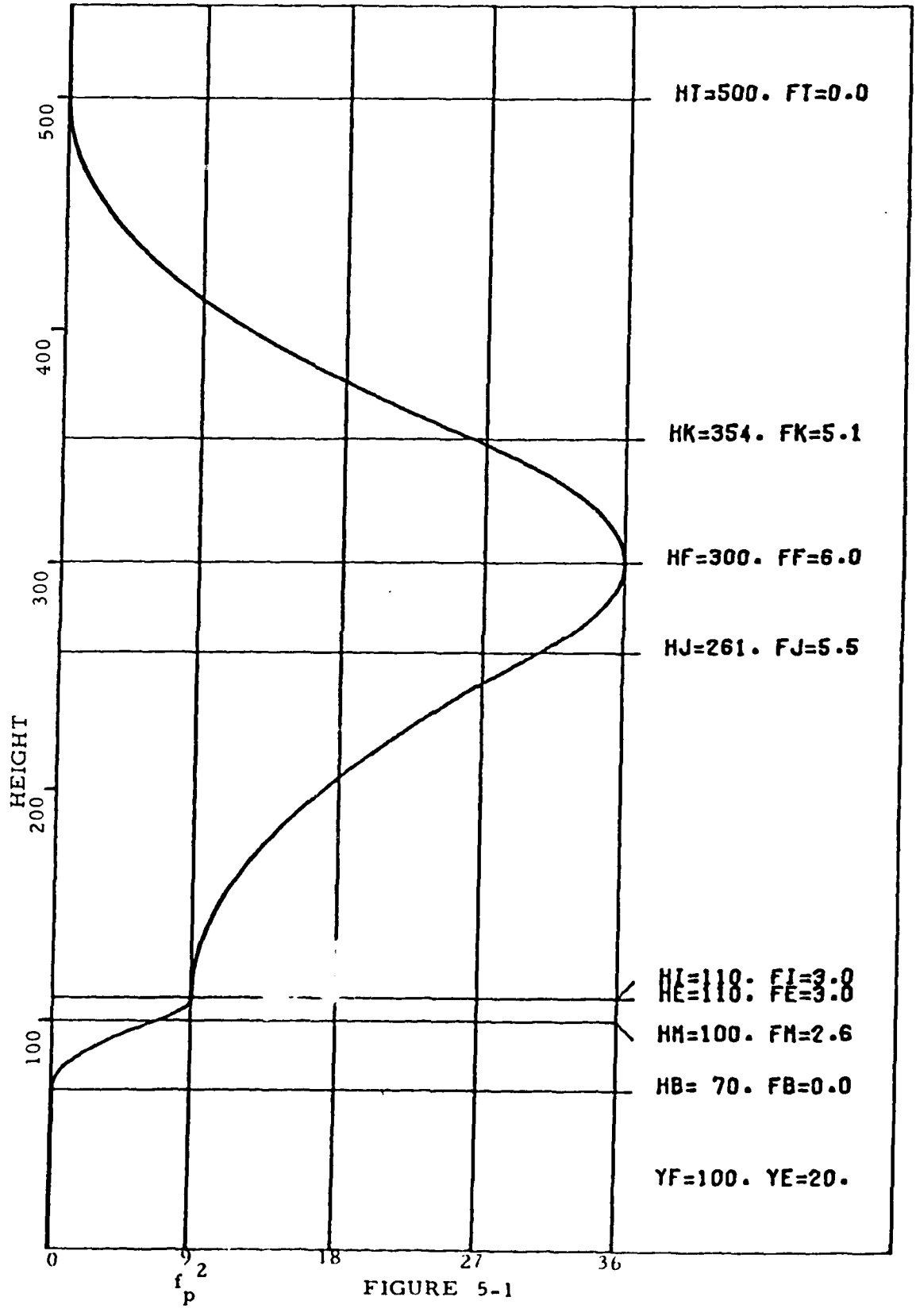

FIGURE 5-1

PSQP Electron Density Profile, $F_L = 1/2\ F_E$

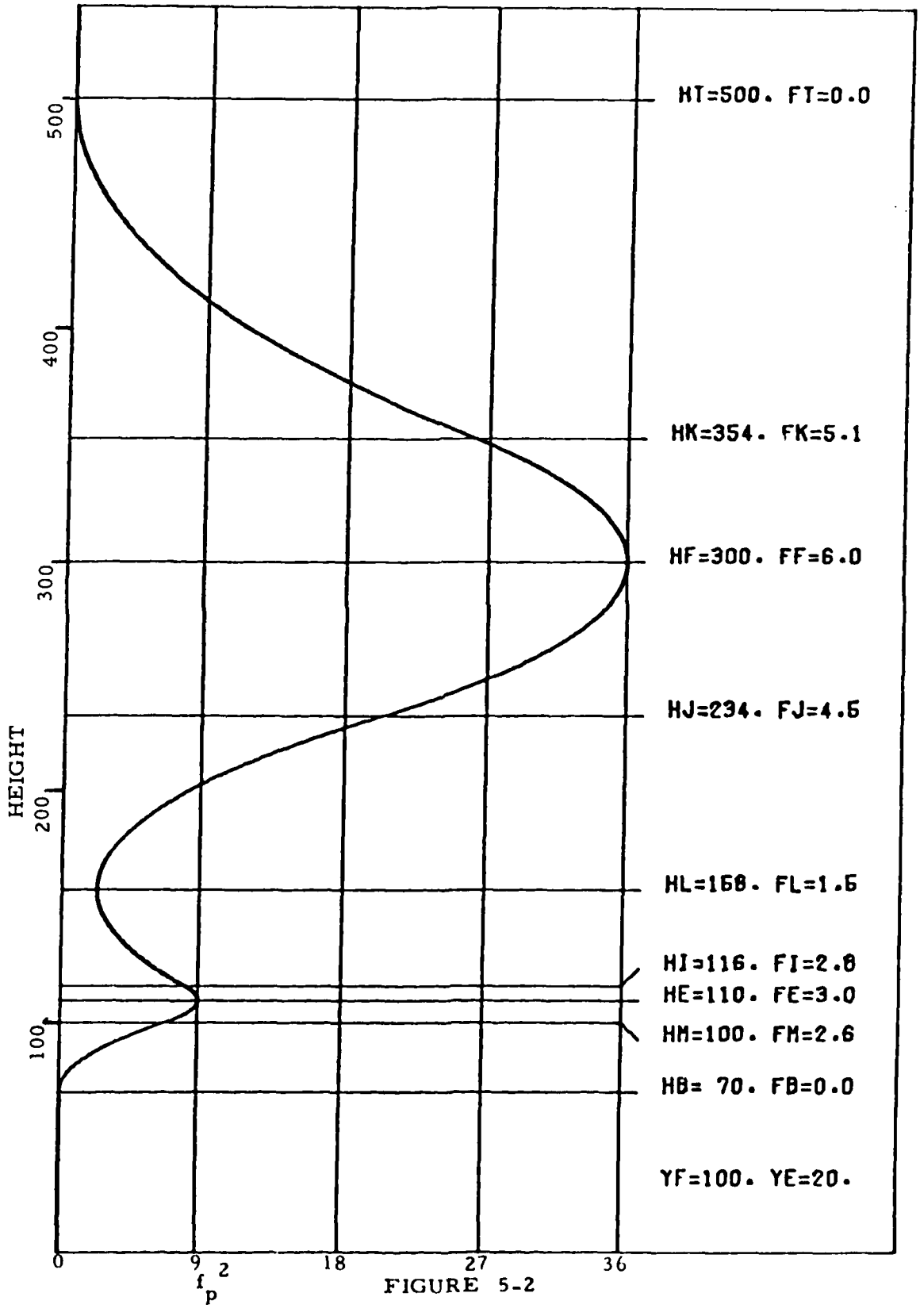

FIGURE 5-2

PSQP Electron Density Profile, $F_L = 0$

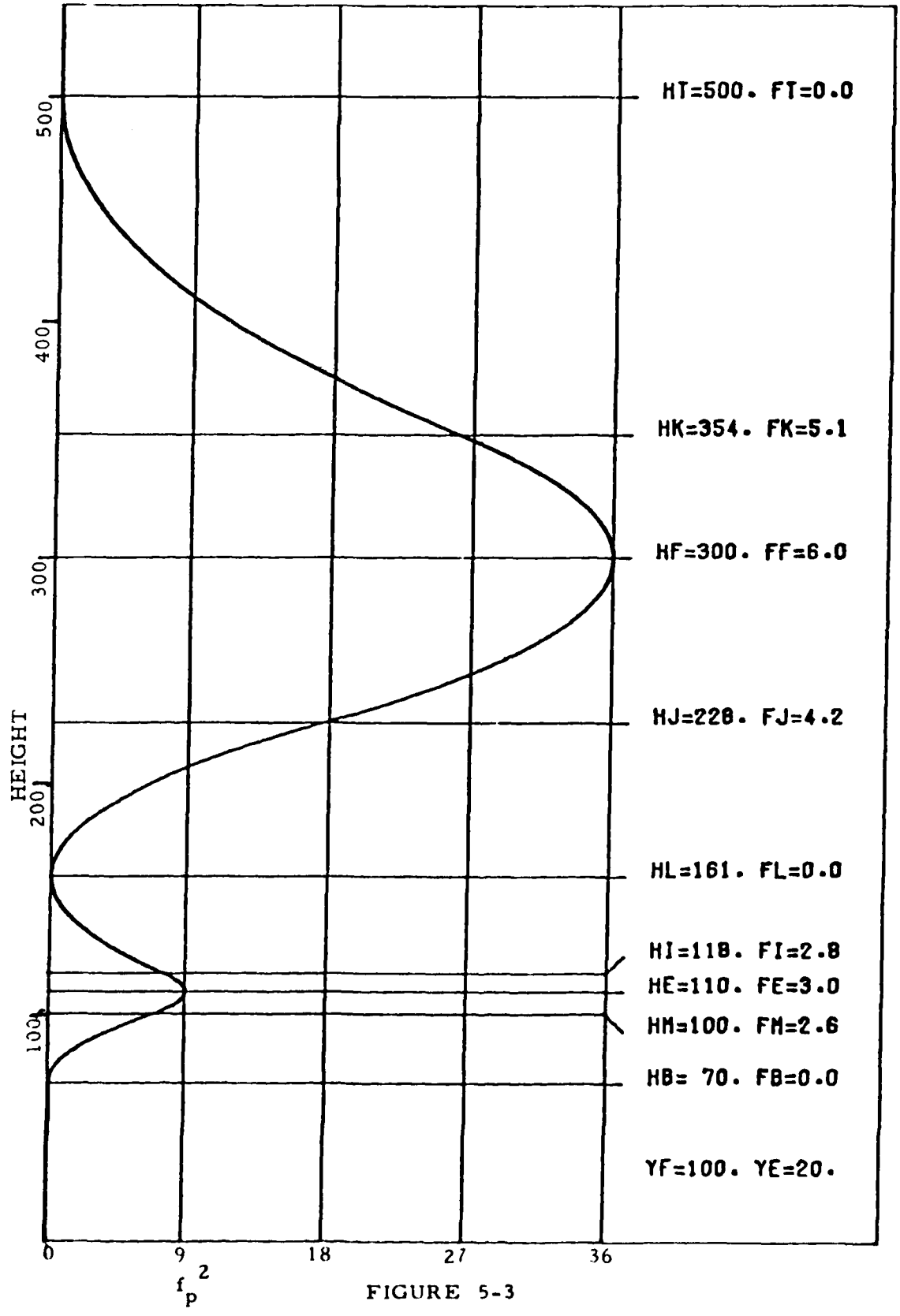

FIGURE 5-3

PSQP Electron Density Profile, $F_j = 1.7\ F_E$

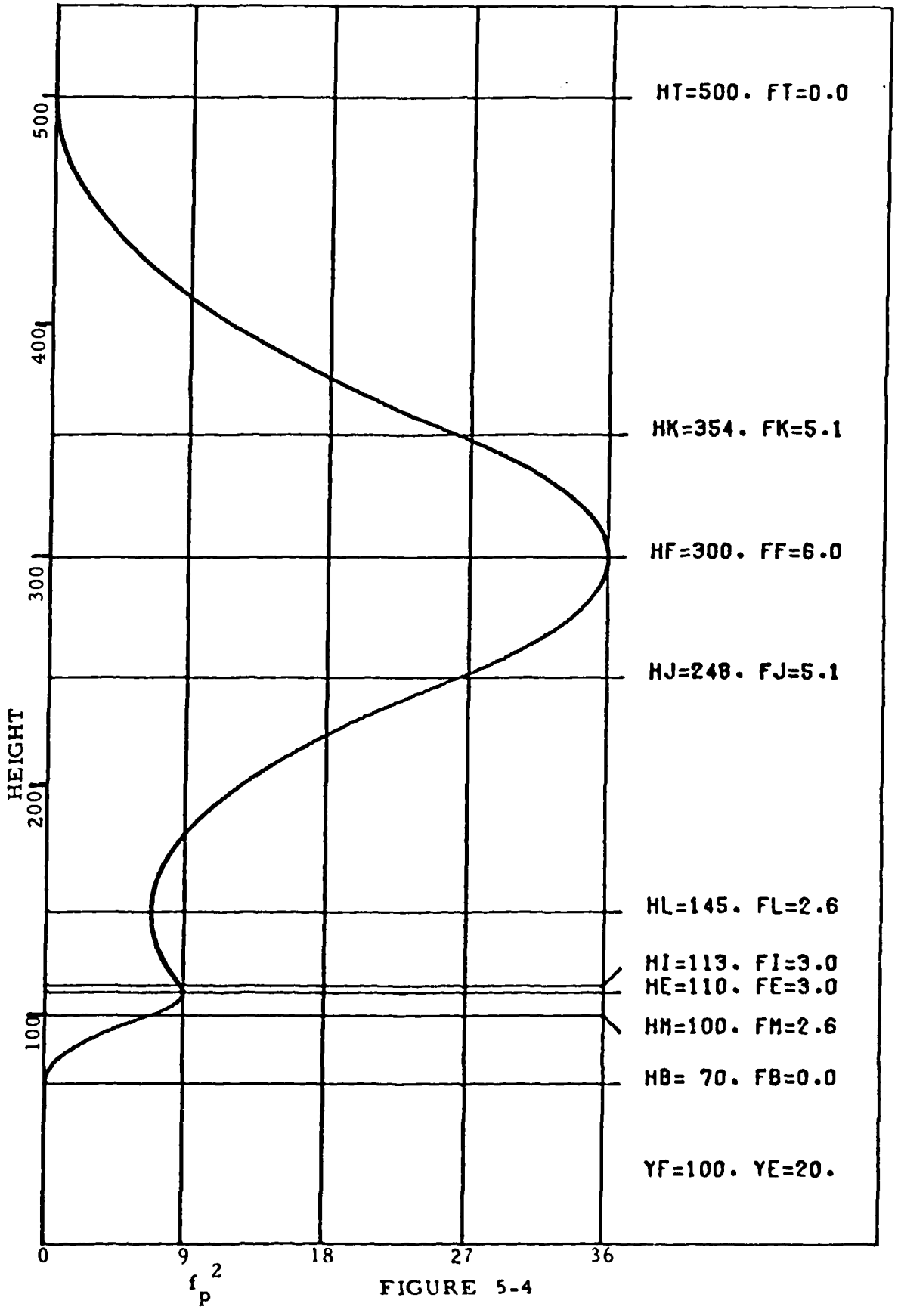

FIGURE 5-4

6. IONOSPHERIC LAYER MODELS AND ELECTRON DENSITY PROFILES

A computer program has been written which performs the integration of the ray equations through quasi-parobolic ionospheric layers. The primary source of models for the individual ionospheric layers used in this Fast Ionospheric Modeling Program (FIMP) is the ITS model providing sets of numerical coefficients for the evaluation of f_oF_2, $M(3000)F_2$, $h'F_2$ and f_oE. Each ionospheric characteristic is represented for a given month and solar activity by quasi orthogonal-polynomial expressions in terms of geographic latitude, geographic longitude, and coordinated universal time. Detailed descriptions of this model are found in the literature [14, 15, 16, 17, 18].

This model of ionospheric characteristics only purports to provide monthly median values of the individual parameter; on any given day deviations up to 20% can be expected. The FIMP program expects input data taken from a recent vertical ionogram from which the model characteristics may be updated to more nearly reflect the actual ionospheric conditions prevailing at the time for which the simulation study is being constructed.

The updating process employed is quite simple: if P_o is the observed value of a given ionospheric parameter extracted from the vertical ionogram, and P_m is the model value of that parameter at the time and place of the vertical ionogram, then a correction factor $k_p = P_o/P_m$ is evaluated. Subsequently, when that parameter P_m is extracted from the model at some other (nearby) time and place, the parameter is updated to the value given by $P_u = k_p P_m$.

At the beginning of a run of the FIMP program, information from the vertical and oblique ionograms are input, and a table of required ionospheric characteristics is constructed along the great circle defined by the transmitter and its boresight azimuth.

Information from the oblique ionogram may also be used to correct the ionospheric characteristics model, in the sense of constructing a down range model of f_oF_2 constrained to reproduce the leading edge of the oblique ionogram.

This technique utilizes the initial climatological variation of all parameters except for f_oF_2. Information from the oblique ionogram is input to the FIMP program as a list of (one way) group paths corresponding to a set of equally spaced frequencies. Initially f_oF_2 is established by the updated model as well as the other parameters of the synthetic ionospheric profile. The first frequency in the set is selected.

The minimum group path corresponding to that frequency f_o in that synthetic profile characterized by $f_oF_2 = f_{co}$ is calculated and compared with the corresponding group path of the leading edge. In general these two values would not agree; assume that the simulated minimum group path is larger than the leading edge group path.

The simulated minimum group path, in this case, would be appropriate on the actual oblique ionogram for a larger frequency f_x than the operating frequency f_o. This frequency f_x may be determined from interpolation within the array of leading edge group paths.

The discrepancy between simulated and observed group paths is now ascribed to an error in the value of f_c in the synthetic profile; in this

example f_c is too small and should be increased. A new value of critical frequency is then defined by

$$f_c = f_c \, f_x / f_o \quad ,$$

and the process is iterated until the discrepancy between simulated and observed group paths is small (less than 0.5 km).

The limit of this iterative process results in a value of the critical frequency f_c which is then presumed to be the appropriate value of f_oF_2 at the reflection point of the simulated minimum group path. As the frequencies in the defined set are so processed, a function f_oF_2 versus range from transmitter is developed which reproduces the leading edge of the oblique ionogram within the established tolerance.

However, this function, despite its ability to reproduce the leading edge so well, is not considered reliable in detail, but is considered reliable to provide the down range trends of f_oF_2. The results of the previous analysis are fitted to a straight line constrained to fit the updated model at the transmitter location. Furthermore, only elements of the function at ranges exceeding 1000 kilometers are employed in the fitting procedure. This linear model for f_oF_2 is then employed in a simulation of the leading edge, discrepancies from the observed ionogram are taken as reliability estimates of the FIMP system. The linear model is further employed in further range registration calculations desired by the user for the current program run.

The electron density profile chosen for the FIMP ray calculation program is a piecewise smooth quasiparabolic model based upon f_oE, f_oF_2, h_mF_2, and y_mF_2 being modeled from the global ionospheric characteristic

model. The layers consist of (1) an inverted QP "D" layer attached to the E layer at the 100 km level falling smoothly to zero below that level, (2) a QP E-layer at a layer height 100 km and semithickness 20 km, (3) an inverted QP layer attached between the E and F layer according to the scale independent criterior established in Section 5, and (4) a QP F layer. In addition, the ray on the way down may encounter a different E-layer from that on the way up.

Since each ray in the frequency-elevation angle family probes in general a different region of the ionosphere each such ray requires a different profile. The profile, then, is synthesized from f_oE for the upward track taken at the point of joining the intermediate layer, f_oE for the downward track similarly chosen, and the F layer parameters chosen at the reflection point. Because the solution for these points are known a posteriori, the final solution is approached in an iterative fashion. This iteration does converge rapidly, especially if care is exercised to select a frequency-elevation member of the ray family close to the most recently completed ray calculation.

7. APPLICATIONS TO TRANSMISSION CIRCUITS

One of the most common applications of ionospheric ray tracing programs is the determination of the circuit parameters (transmission frequency, f and elevation angle, β) required for communication between given transmitter and receiver locations. For an arbitrarily specified ionosphere this usually involves the use of a homing algorithm with a three dimensional ray tracing program. When the electron density gradients are large even this technique does not yield unique results and the computer time required to find any possible circuits may be quite large. If an analytic expression for the range in terms of f and β can be used the problem may be greatly simplified. The quasi-parabolic model has been used to obtain solutions to the homing problem for several ionospheric models. The results we presented include those with several layers but neglect the effects of the horizontal gradients.

The simplest case is that of a single F_2 layer (SLQP night time ionosphere) when the ionosphere is entirely specified by f_oF_2, h_mF_2 and y_mF_2. We characterize the transmission curves by the ratio of the transmission frequency f, to f_oF_2 : $F \equiv f/f_oF_2$.
The ground is given by the following expression,

$$R = 2a \left\{ (\gamma-\beta) - F \frac{a \cos\beta}{2\sqrt{C}} \log_e \left(\frac{Ur_b^2}{w^2} \right) \right\}$$

where $$C = \left(\frac{r_b r_m}{y_m} \right)^2 - F^2 a^2 \cos^2\beta$$

$$A = F^2 - 1 + \left(\frac{r_b}{y_m}\right)^2$$

$$B = -2\, r_m \left(\frac{r_b}{y_m}\right)^2$$

$$U = B^2 - 4AC$$

$$W = 2\sqrt{C}\; F\, r_b \sin\gamma + 2C + B\, r_b$$

$$\cos\gamma = \frac{a}{r_b}\cos\beta \quad , \quad \gamma \text{ is the elevation}$$

angle at the base of the ionosphere

$$r_m = a + h_m F_2$$

$r_b = r_m - y_m F_2$ and a is the radius of the earth.

The group path, P' is given by

$$P' = 2\left\{1 - F^2/A\right\} r_b \sin\gamma - 2a\sin\beta - \frac{BF}{2A^{3/2}}\log_e\left(\frac{U}{V}\right)$$

where $V = 2Ar_b + B + 2\, r_b F\sqrt{A}\sin\gamma$.

Figures 7-1 and 7-2 show the ground range and group path for a sample ionosphere with $h_m F_2$ = 325 km. and $y_m F_2$ = 175 km. The elevation angles are sampled at 1° intervals for F values between 0.2 and 3.0 at intervals of 0.2. The determination of the circuit parameters for a specified range R_o consists in finding the solutions of the equation

$$R_o = R(F, \beta)$$

We first find the solution for the smallest possible elevation angle. There are two cases:

i) Specular reflection from the bottom of the ionosphere,

$$F = 0^+ \qquad \beta_{min} = \tan^{-1}\left\{\frac{\cos\left(R_o/2a\right) - a/r_b}{\sin\left(R_o/2a\right)}\right\}$$

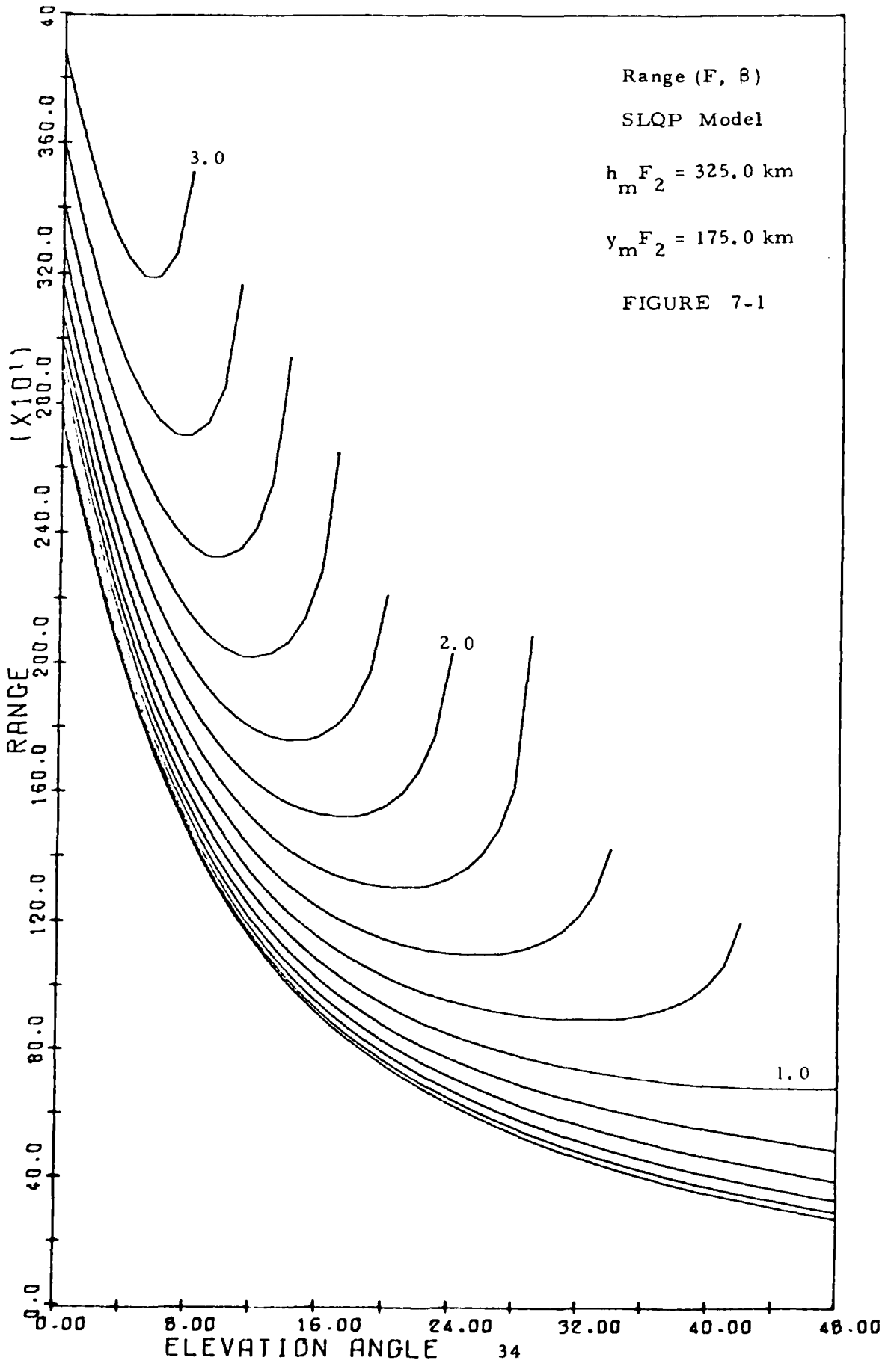
Range (F, β)
SLQP Model
$h_m F_2$ = 325.0 km
$y_m F_2$ = 175.0 km
FIGURE 7-1
RANGE (X10¹)
ELEVATION ANGLE
0.0
40.0
80.0
120.0
160.0
200.0
240.0
280.0
320.0
360.0
400
0.00
8.00
16.00
24.00
32.00
40.00
48.00
3.0
2.0
1.0

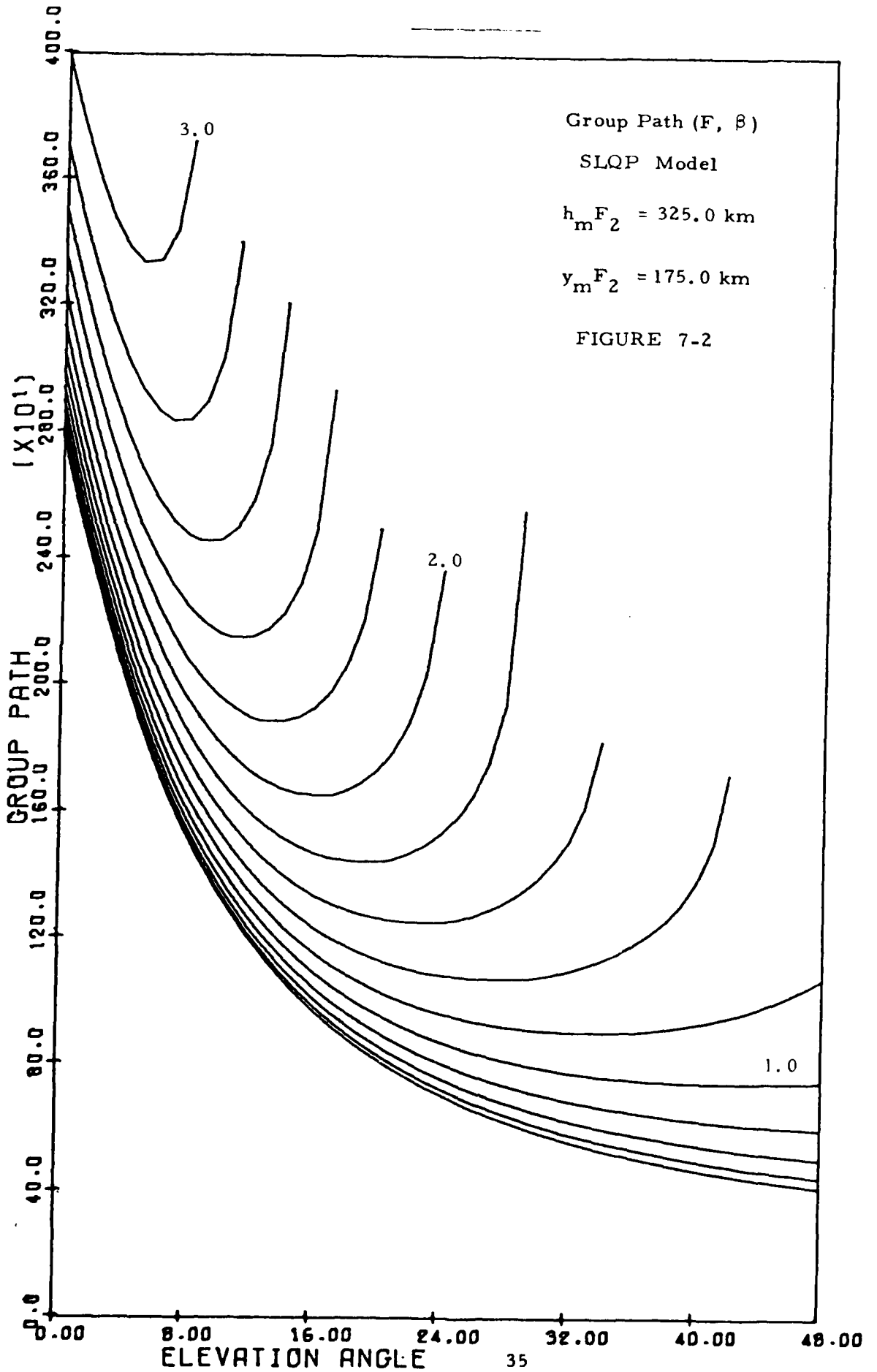
Group Path (F, β)
SLQP Model
h_mF_2 = 325.0 km
y_mF_2 = 175.0 km
FIGURE 7-2
3.0
2.0
1.0
GROUP PATH (X10¹)
400.0
360.0
320.0
280.0
240.0
200.0
160.0
120.0
80.0
40.0
0.0
0.00
8.00
16.00
24.00
32.00
40.00
48.00
ELEVATION ANGLE

ii) $F \neq 0 \qquad \beta_{min} = 0^\circ$.

Other solutions are then searched for at elevation angles greater than β_{min} for a given angular step size. For each new elevation angle an iterative procedure is used starting with the value of F found as a solution for the previous angle. A correction to this F is found using:

$$\Delta F_i = \frac{(R(F_i, B) - R_o)}{\frac{\partial R}{\partial F}(F_i, \beta)}$$

$$F_i+1 = F_i+\Delta F_i$$

where $\frac{\partial R}{\partial F}$ is calculated analytically using

$$\frac{\partial R}{\partial F} = \frac{a \cos\beta}{2\sqrt{C}} \left\{ \log_e \left(\frac{U r_b^2}{W^2}\right) \left[\frac{F}{2C} \frac{\partial C}{\partial F} - 1\right] - \frac{F W^2}{U} \left[\frac{1}{W^2} \frac{\partial U}{\partial F} - \frac{2 U}{W^3} \frac{\partial W}{\partial F}\right] \right\}$$

where

$$\frac{\partial C}{\partial F} = -2Fa^2 \cos^2\beta$$

$$\frac{\partial U}{\partial F} = -4 C \frac{\partial A}{\partial F} + A \frac{\partial C}{\partial F}$$

$$\frac{\partial A}{\partial F} = 2 F \qquad \text{and}$$

$$\frac{\partial W}{\partial F} = 2\sqrt{C}\ r_b \sin\gamma + \left(F \frac{r_b \sin\gamma}{\sqrt{C}} + 2\right) \frac{\partial C}{\partial F}$$

We search for solutions for a given range in 1/4° steps in elevation angle

between β_{min} and β_{max}, the angle at which the ray penetrates the maximum height of the layer. This occurs where $U \equiv 0$ which yields

$$\beta_{max} = \cos^{-1}\left\{\frac{1}{Fa}\left[\left(\frac{r_b\, r_m}{y_m}\right)^2 - \frac{B^2}{4A}\right]^{1/2}\right\}$$

For this sampling internal the procedure converges rapidly using the starting frequency of the previous angle. For a given range the solutions include the low rays, the high rays and the MUF. Figure 7-3 shows all the solutions obtained for a 3000 km path using the sample set of ionospheric parameters whose transmission curves where shown in Figure 7-1. We have considered propagation by up to four hop ionospheric modes. The first hop starts from initial condition ii), while the solutions for the other three hops were obtained beginning with initial condition i). For each pair of circuit parameters on the curves we calculate the group path. The resulting bistatic ionogram is plotted as a function of the normalized frequency, F in Figure 7-4. In a particular application one would only consider that part of the ionogram that would be possible for the given transmitter antenna pattern. While we do not explicitly account for the effects of horizontal gradients in the ionogram it is possible to obtain some indication of the size of these effects by considering other stratified ionospheric layers with parameters that are slightly different from the original problem. For the test ionosphere this might include a range of 300-350 km for $h_m F_2$, and 150-200 km for $y_m F_2$.

When we use a multi-layer quasi-parabolic model (MLQP) we have in addition to the F_2 layer parameters, three other parameters for the underlying ionization of the F layer. We have taken constant values of

FIGURE 7-3

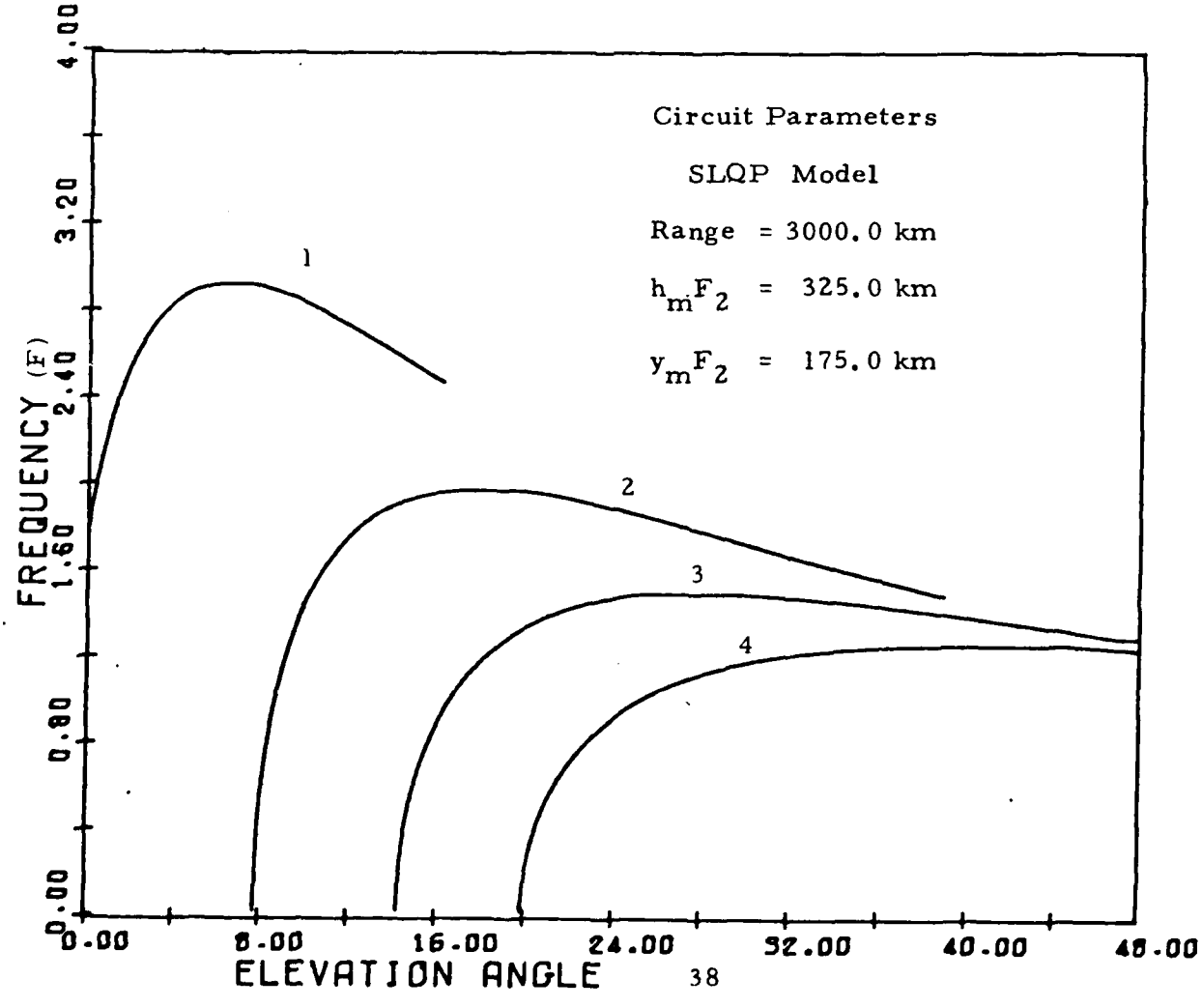
Circuit Parameters
SLQP Model
Range = 3000.0 km
h_mF_2 = 325.0 km
y_mF_2 = 175.0 km
1
2
3
4
FREQUENCY (F)
4.00
3.20
2.40
1.60
0.80
0.00
0.00
8.00
16.00
24.00
32.00
40.00
48.00
ELEVATION ANGLE

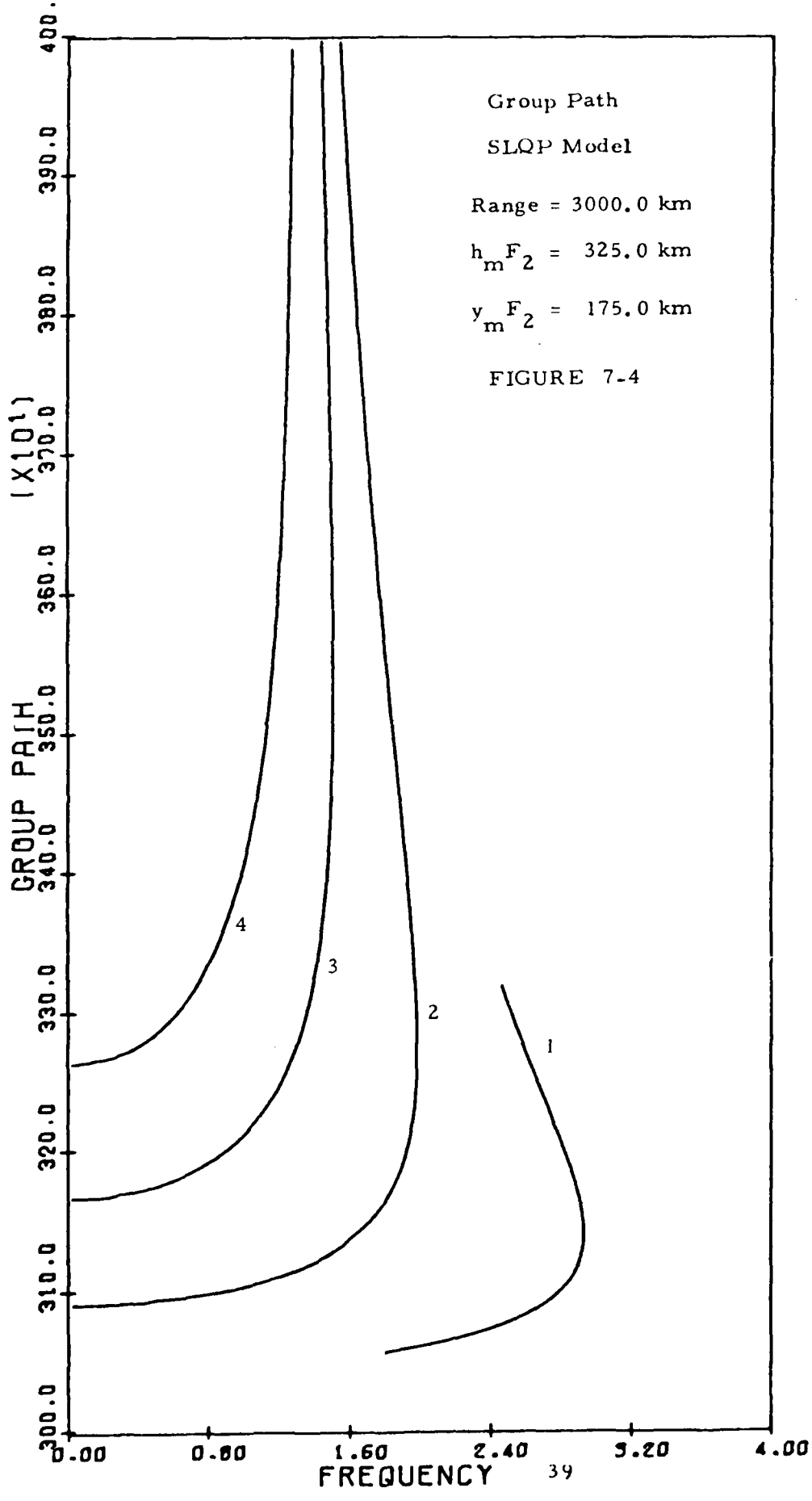
Group Path
SLQP Model
Range = 3000.0 km
h_mF_2 = 325.0 km
y_mF_2 = 175.0 km
FIGURE 7-4
GROUP PATH (X10¹)
400.0
390.0
380.0
370.0
360.0
350.0
340.0
330.0
320.0
310.0
300.0
0.00
0.80
1.60
2.40
3.20
4.00
FREQUENCY
1
2
3
4

110 km and 20 km for the height, h_mE and semithickness, y_mE of the E layer and examine the effect of various values of f_oE upon the transmission curves. In Figure 7-5 we show the vertical electron density distribution obtained for various combinations of the layer parameters. We have fixed h_mF_2 = 325 km for all six profiles. The other parameters used are

	f_oF_2	y_mF_2	f_oE	
(a)	10.0MHz	175. km	3.5MHz	———
(b)	10.0	125.	3.5	· ——— ·
(c)	10.0	100.	3.5	· — — ·
(d)	10.0	175.	2.5	· · · · ·
(e)	7.0	175.	3.5	———
(f)	7.0	125.	3.5	· ——— ·

We have calculated the range and group path for frequency intervals of 2MHz and angular intervals of 1^o for the parameter sets (a)-(e). Figures 7-6 and 7-7 are plots of R and P' for the parameters in (a) and Figures 7-8 through 7-10 are the range curves for parametrs (b), (d) and (e). The maximum frequency that can propagate by the E layer is given by:

$$f_{max}E = \left\{ \frac{a^2}{\left(h_mE\right)^2 + 2a\left(h_mE\right)} \right\}^{1/2} f_oE$$

For case (d) f_oE=2.5MHz and $f_{max}E$=13.4MHz and for all the other cases f_oE=3.5MHz and $f_{max}E$=18.8MHz. The absence of E modes above these frequencies is clearly visible in Figures 7-6 through 7-10. The E and F propagation modes are clearly separated in all of the plots. With a 1^o

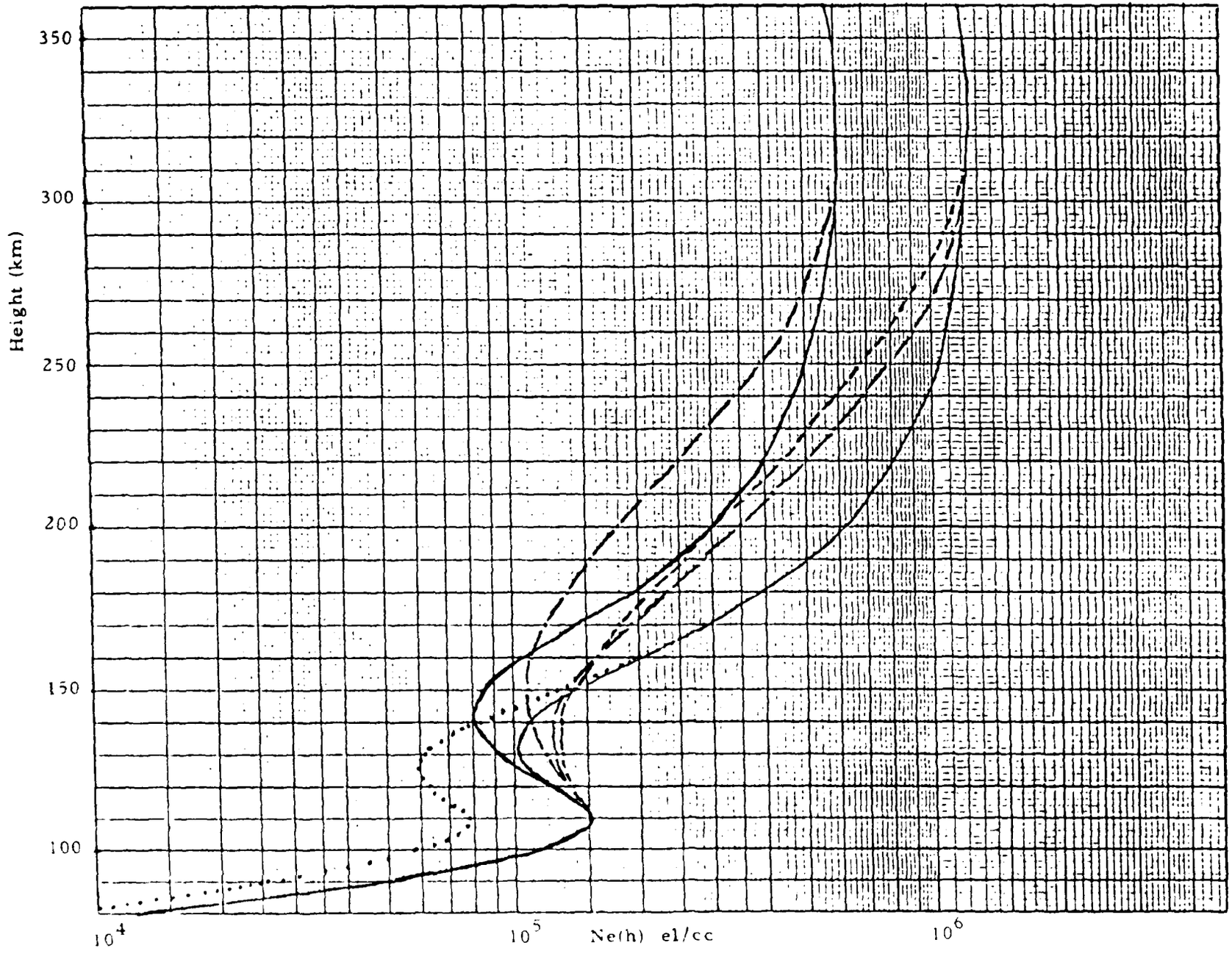

Vertical Electron Density Distribution MLQP

FIGURE 7-5
41

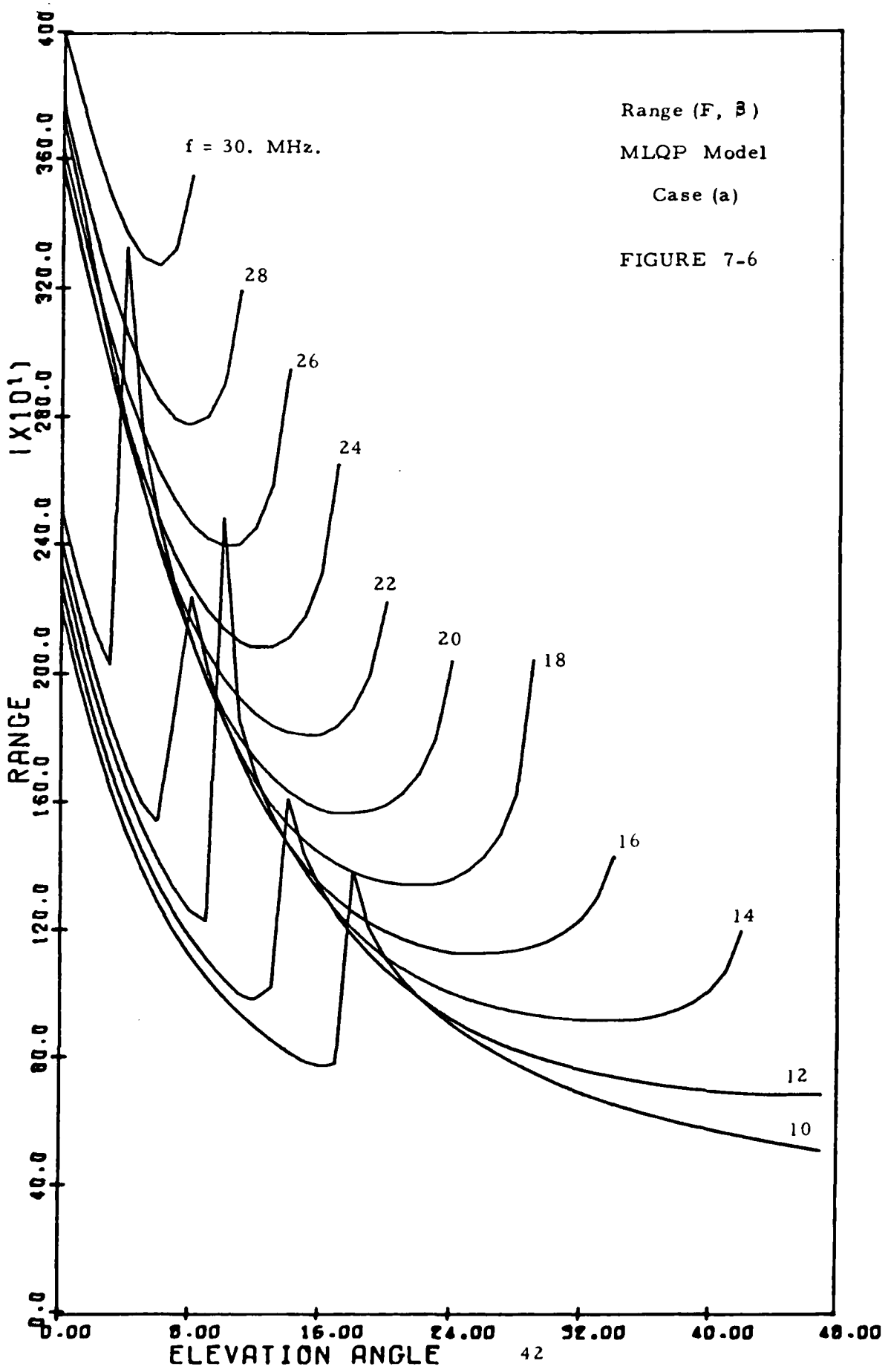
Range (F, β)
MLQP Model
Case (a)
f = 30. MHz.
28
26
24
22
20
18
16
14
12
10
RANGE (X10¹)
400
360.0
320.0
280.0
240.0
200.0
160.0
120.0
80.0
40.0
0.0
0.00
8.00
16.00
24.00
32.00
40.00
48.00
ELEVATION ANGLE

FIGURE 7-6

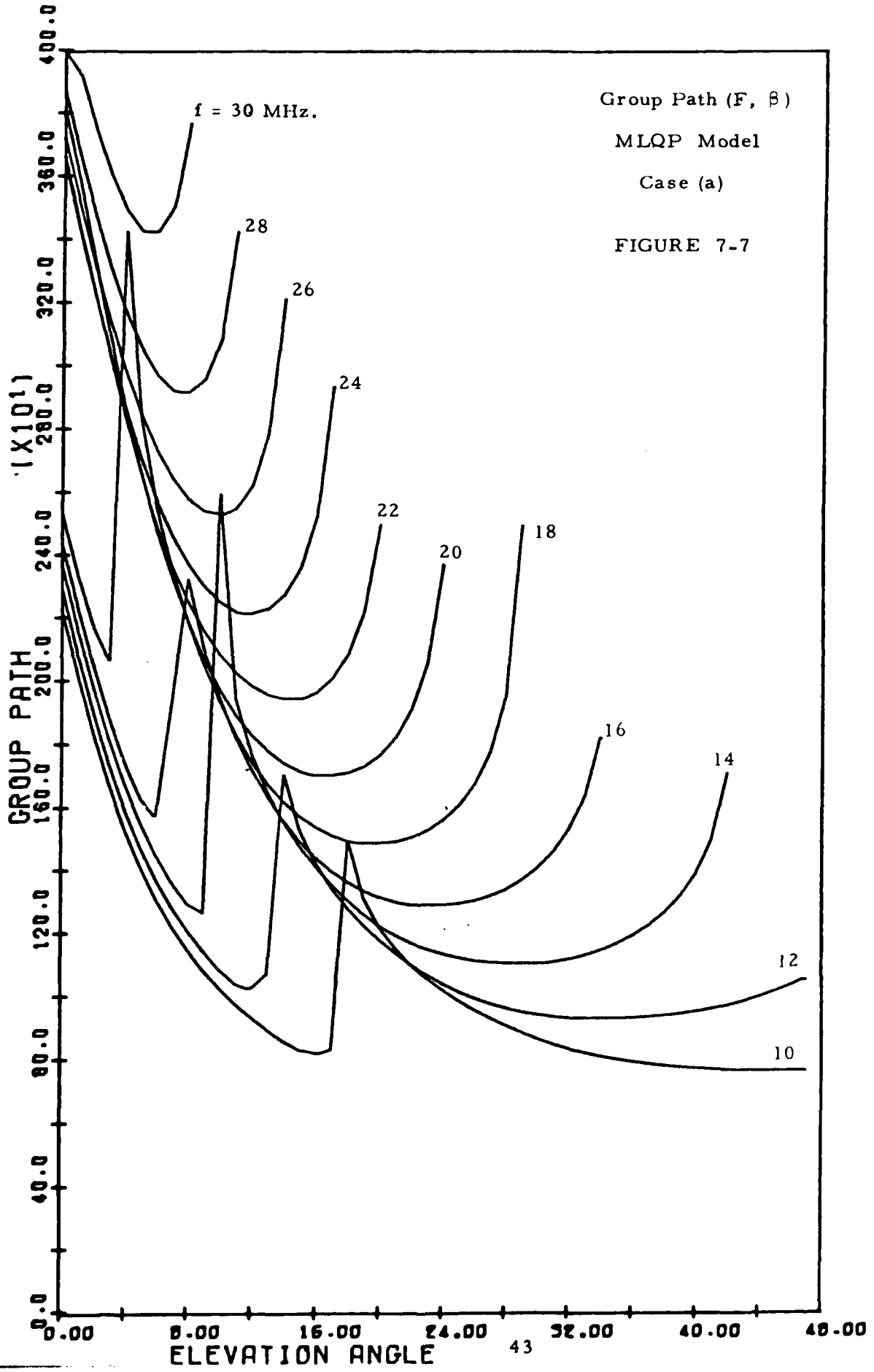
Group Path (F, β)
MLQP Model
Case (a)
f = 30 MHz.
28
26
24
22
20
18
16
14
12
10
GROUP PATH (X10¹)
400.0
360.0
320.0
280.0
240.0
200.0
160.0
120.0
80.0
40.0
0.0
0.00
8.00
16.00
24.00
32.00
40.00
48.00
ELEVATION ANGLE

FIGURE 7-7

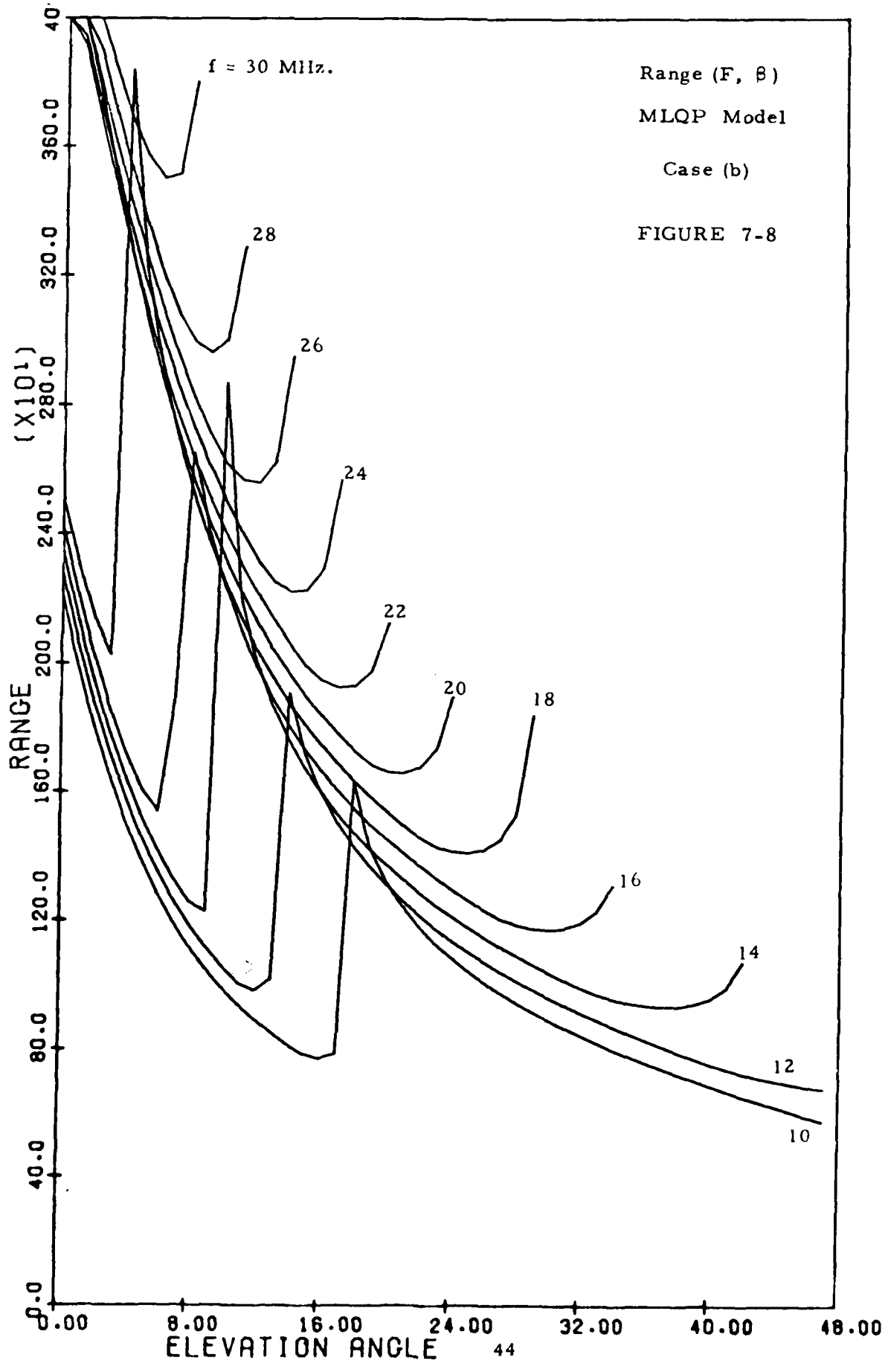

Range (F, β)

MLQP Model

Case (b)

FIGURE 7-8

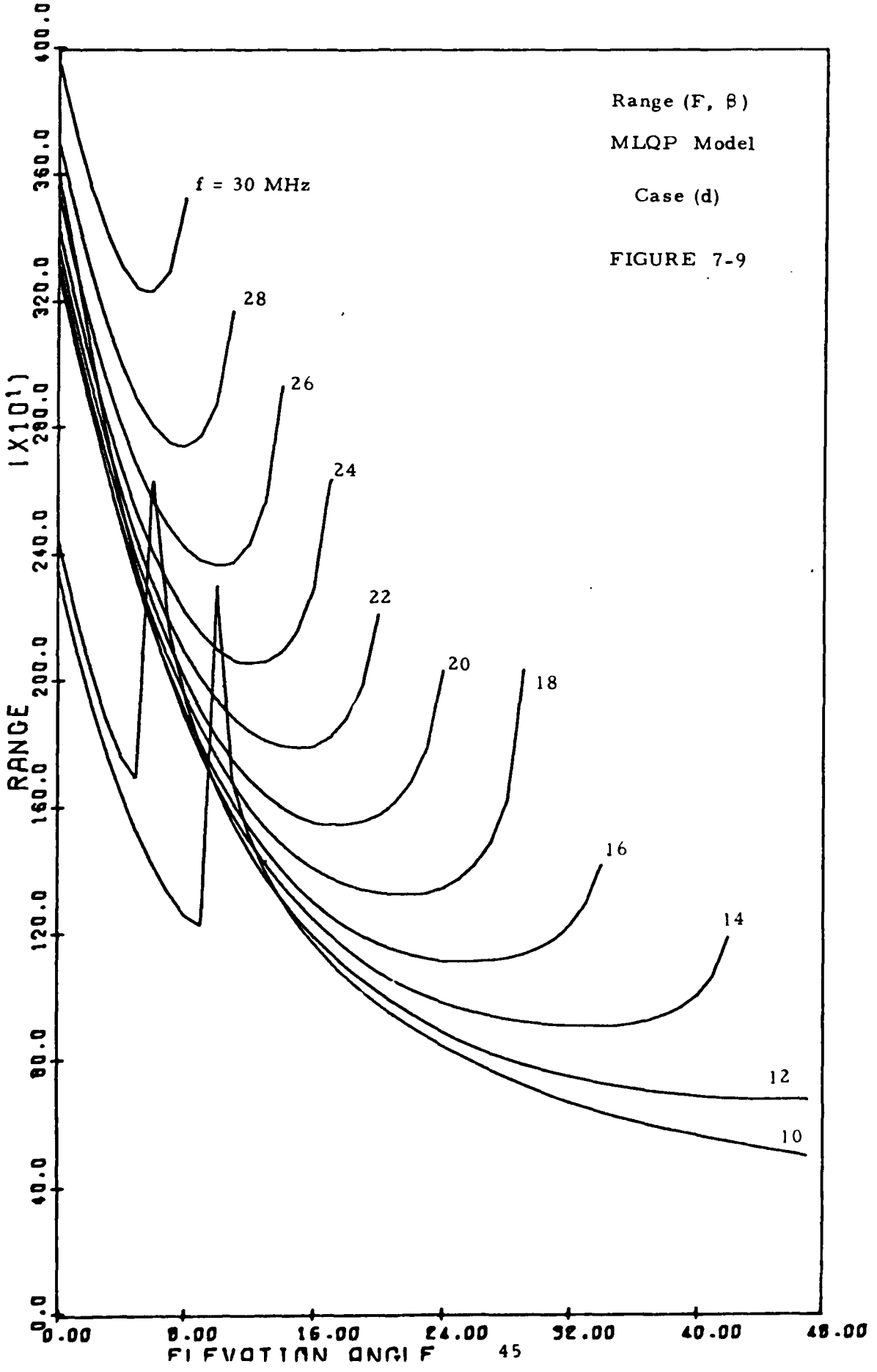
Range (F, β)
MLQP Model
Case (d)
f = 30 MHz
28
26
24
22
20
18
16
14
12
10
RANGE (X10¹)
400.0
360.0
320.0
280.0
240.0
200.0
160.0
120.0
80.0
40.0
0.0
0.00
8.00
16.00
24.00
32.00
40.00
48.00
ELEVATION ANGLE

FIGURE 7-9

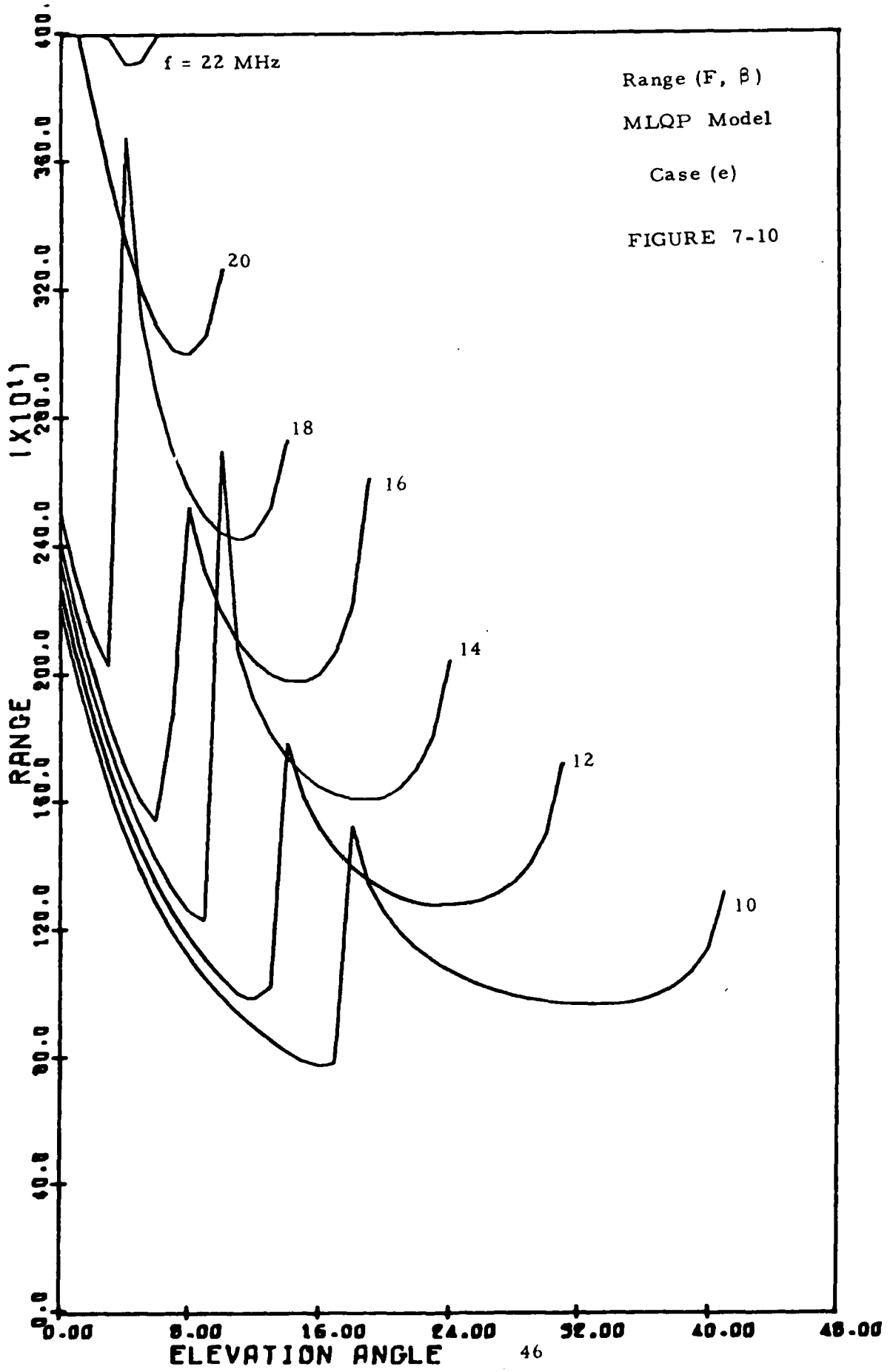
f = 22 MHz
Range (F, β)
MLQP Model
Case (e)
FIGURE 7-10
20
18
16
14
12
10
RANGE (X10¹)
400.
360.0
320.0
280.0
240.0
200.0
160.0
120.0
80.0
40.0
0.0
0.00
8.00
16.00
24.00
32.00
40.00
48.00
ELEVATION ANGLE

sampling interval in β we find only one or two high angle E rays for each set of parameter for any fixed frequency of transmission. A comparison of Figure 7-1 with 7-6 reveals that the E layer has very little effect on the range curves for most of the high rays as we get away from the skip distance. For a fixed frequency we also see from Figure 7-6 and 7-7 that the skip distance and minimum group path do not occur at the same elevation angle.

From Figure 7-3 we see that for the SLQP model if there is a solution to the equation $R_o = R(f, \beta)$ that it is a unique solution. In the case of the MLQP model the crossing of the various frequency curves implies that it is possible to have dual frequency solutions for the same elevation angle for F mode propagation. This complication has lead us to use a different method for finding all the possible solutions for a given range problem. In this case we attempt to find the elevation angle that completes the path for a fixed frequency rather than searching for the frequency for a fixed elevation angle. For each frequency we use the electron density profile to compute the limits on the initial elevation angles for reflection from the different layers. This results in a set of angles:

β_{Emin}	minimum elevation angle for E layer reflection.
β_{Eo}	elevation angle for E layer skip distance.
$\beta_{Emax} = \beta_{Fmin}$	maximum elevation angle for E layer reflection or minimum elevation angle for F layer reflection.
β_{Fo}	elevation angle for F layer skip distance.
β_{Fmax}	maximum elevation angle for F layer reflection (penetration angle).

Between any successive pair of these angles the range curve is a monotonic

function. The range at the end points determines whether a solution exists. A search procedure is then initiated to find the elevation angle which results in a range within a small error of the specified circuit range.

A single method is used to find the appropriate solution even though the function $\frac{\partial R}{\partial \beta}\Big)_f$ has a wide range of variation. The calculation is performed with the variable $\cos^2\beta$ rather than β itself. The ground range is calculated for a $\cos^2\beta_i$ midway between the values at the end points. Depending upon the sign of $(R_o - R(f, \cos^2\beta_i))$ one of the end points is replaced with $\cos^2\beta_i$ and a new midpoint is taken. The procedure is terminated when

$$|R_o - R(f, \cos^2\beta_i)| < 0.5 \text{ km.}$$

Figure 7-11 is a plot of F mode solutions for $R_o = 3000$ km for ionospheric model (a). Figure 7-12 is a plot of the group path as a function of frequency for these solutions. These curves corresponds to the same ionosphere parameters that were used in the SLQP model with the addition of an underlying E layer. Comparing Figure 7-11 with Figure 7-3 we see that most of circuit parameters for rays above the MUF for each hop coincide with each other for the two ionospheric models. For the MLQP model we only searched for solutions for $f \geq f_oF_2$. The effect of changing individual model parameters upon the propagation parameters and the resulting bistatic ionogram for the F modes is shown on Figures 7-13 through 7-16. In Figures 7-13 and 7-14 only the semithickness of the F_2 layer has been changed (case (b)) while in Figures 7-15 and 7-16 (case (d)) the value of f_oE has been changed from 3.5MHz to 2.5MHz. Both changes have very little effect on the propagation above the F layer MUF's. Reducing the

FIGURE 7-11

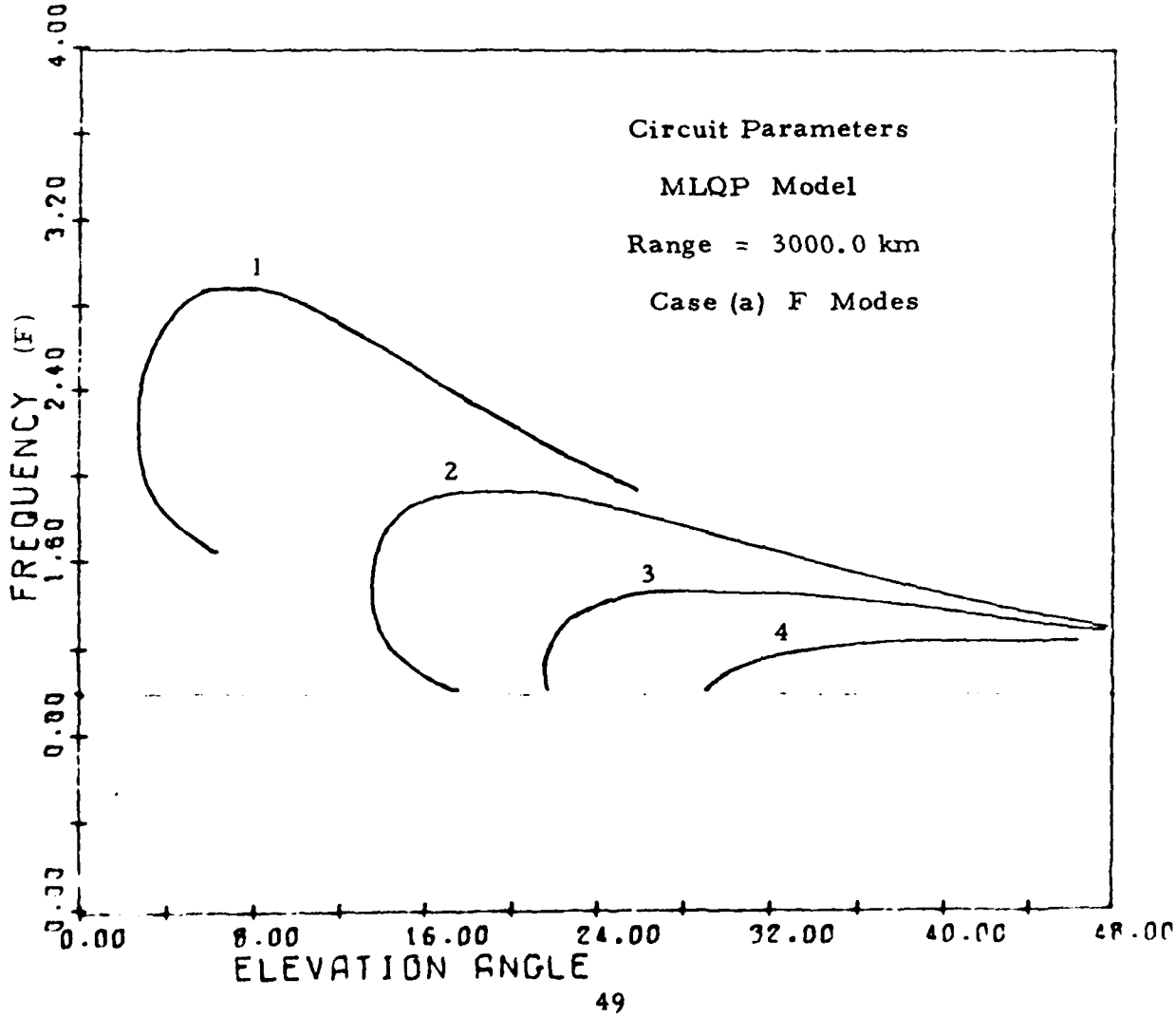
Circuit Parameters
MLQP Model
Range = 3000.0 km
Case (a) F Modes
1
2
3
4
FREQUENCY (F)
4.00
3.20
2.40
1.60
0.80
0.00
0.00
8.00
16.00
24.00
32.00
40.00
48.00
ELEVATION ANGLE

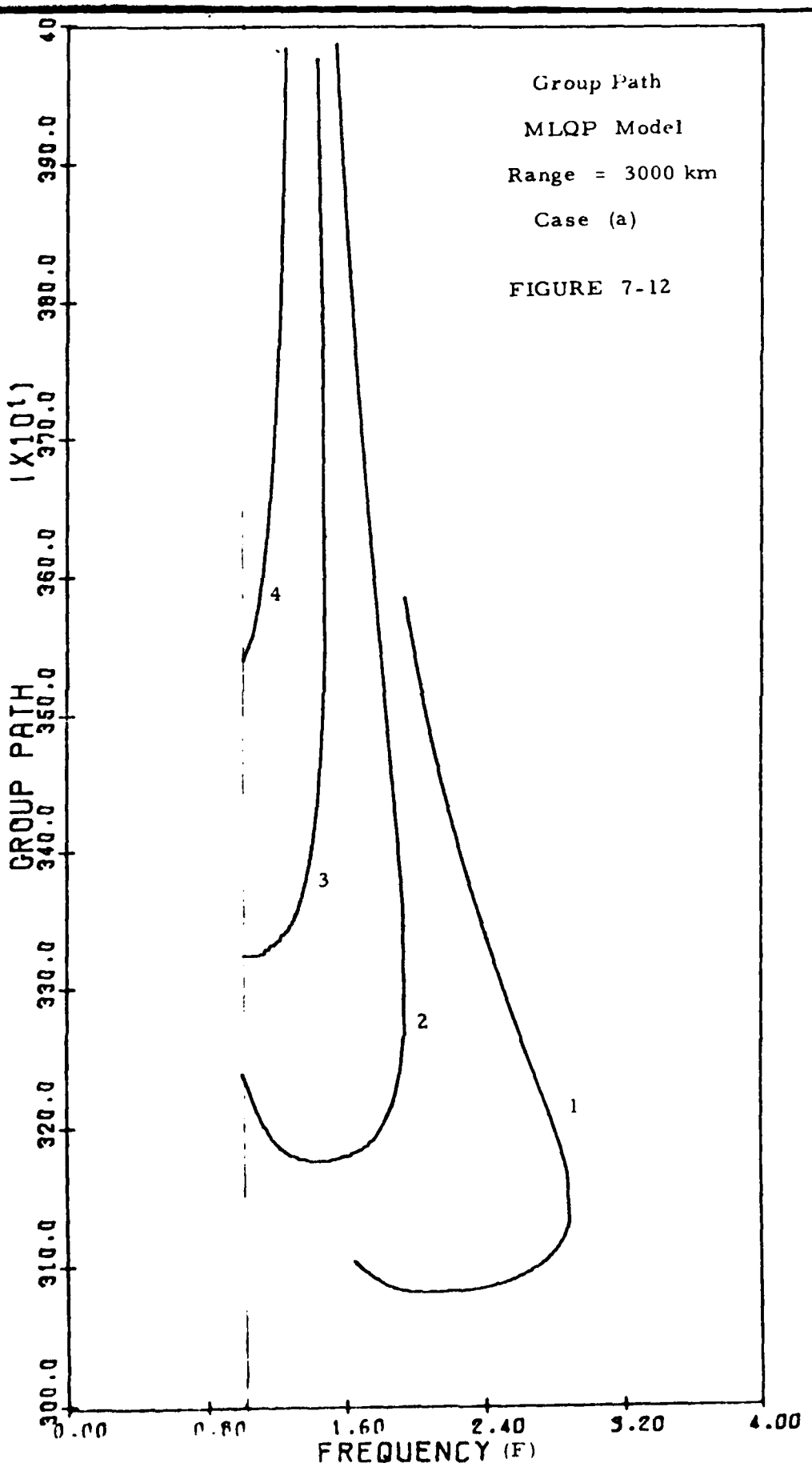
Group Path
MLQP Model
Range = 3000 km
Case (a)
FIGURE 7-12
GROUP PATH (X10¹)
400.0
390.0
380.0
370.0
360.0
350.0
340.0
330.0
320.0
310.0
300.0
0.00
0.80
1.60
2.40
3.20
4.00
FREQUENCY (F)
1
2
3
4

FIGURE 7-13

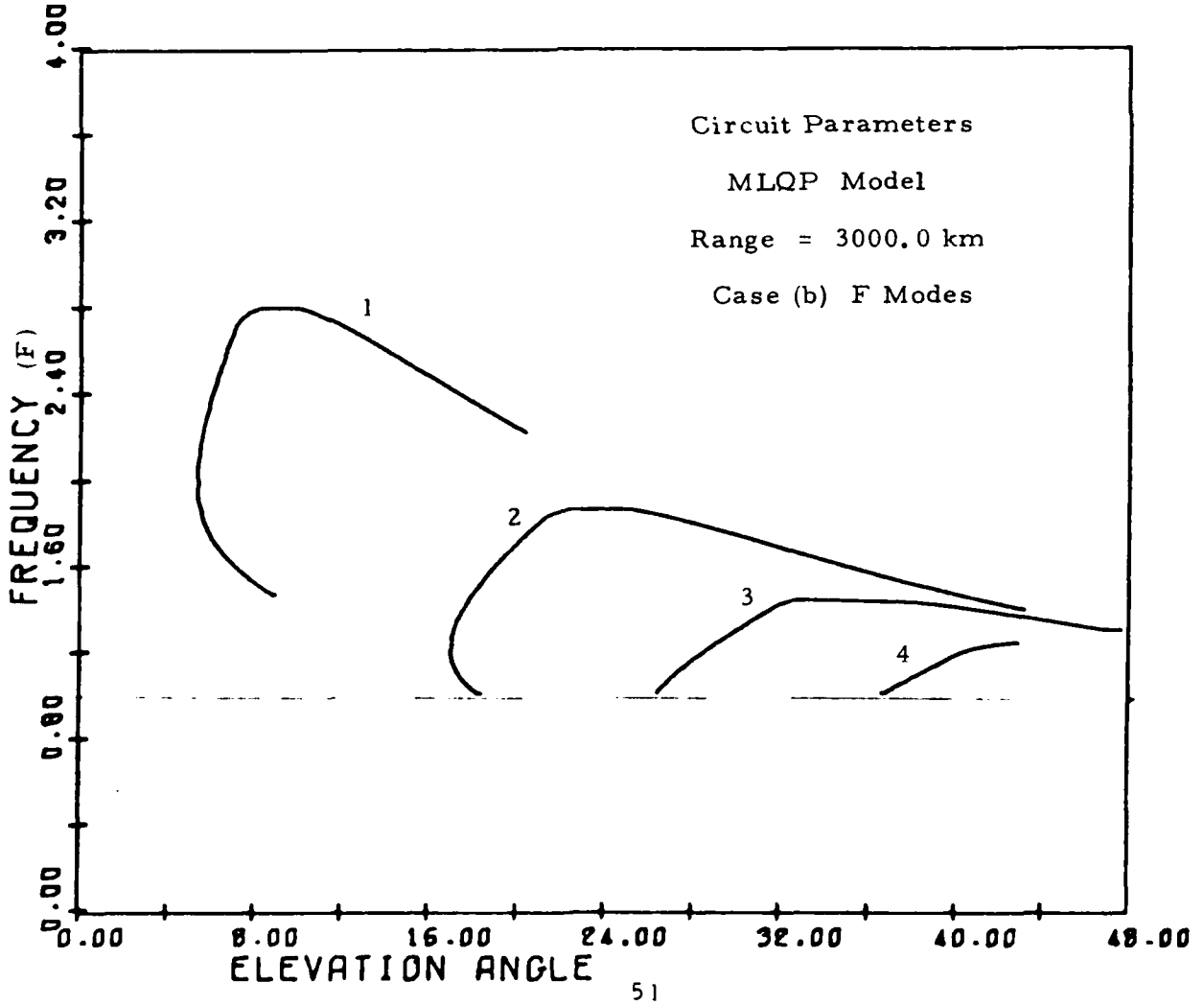
Circuit Parameters
MLQP Model
Range = 3000.0 km
Case (b) F Modes
1
2
3
4
FREQUENCY (F)
4.00
3.20
2.40
1.60
0.80
0.00
0.00
8.00
16.00
24.00
32.00
40.00
48.00
ELEVATION ANGLE

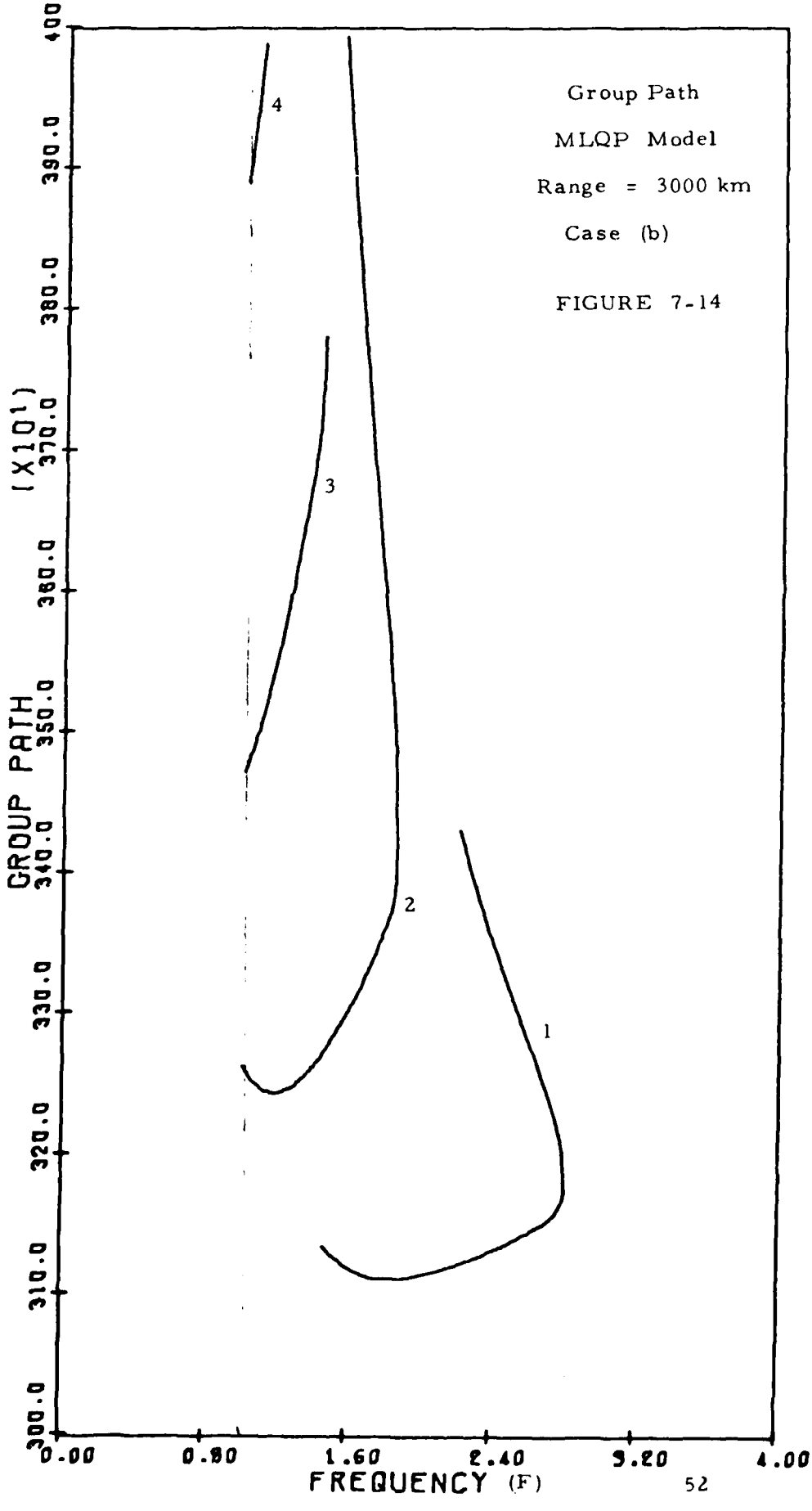
Group Path
MLQP Model
Range = 3000 km
Case (b)
FIGURE 7-14
GROUP PATH (X10¹)
400
390.0
380.0
370.0
360.0
350.0
340.0
330.0
320.0
310.0
300.0
0.00
0.80
1.60
2.40
3.20
4.00
FREQUENCY (F)
1
2
3
4

FIGURE 7-15

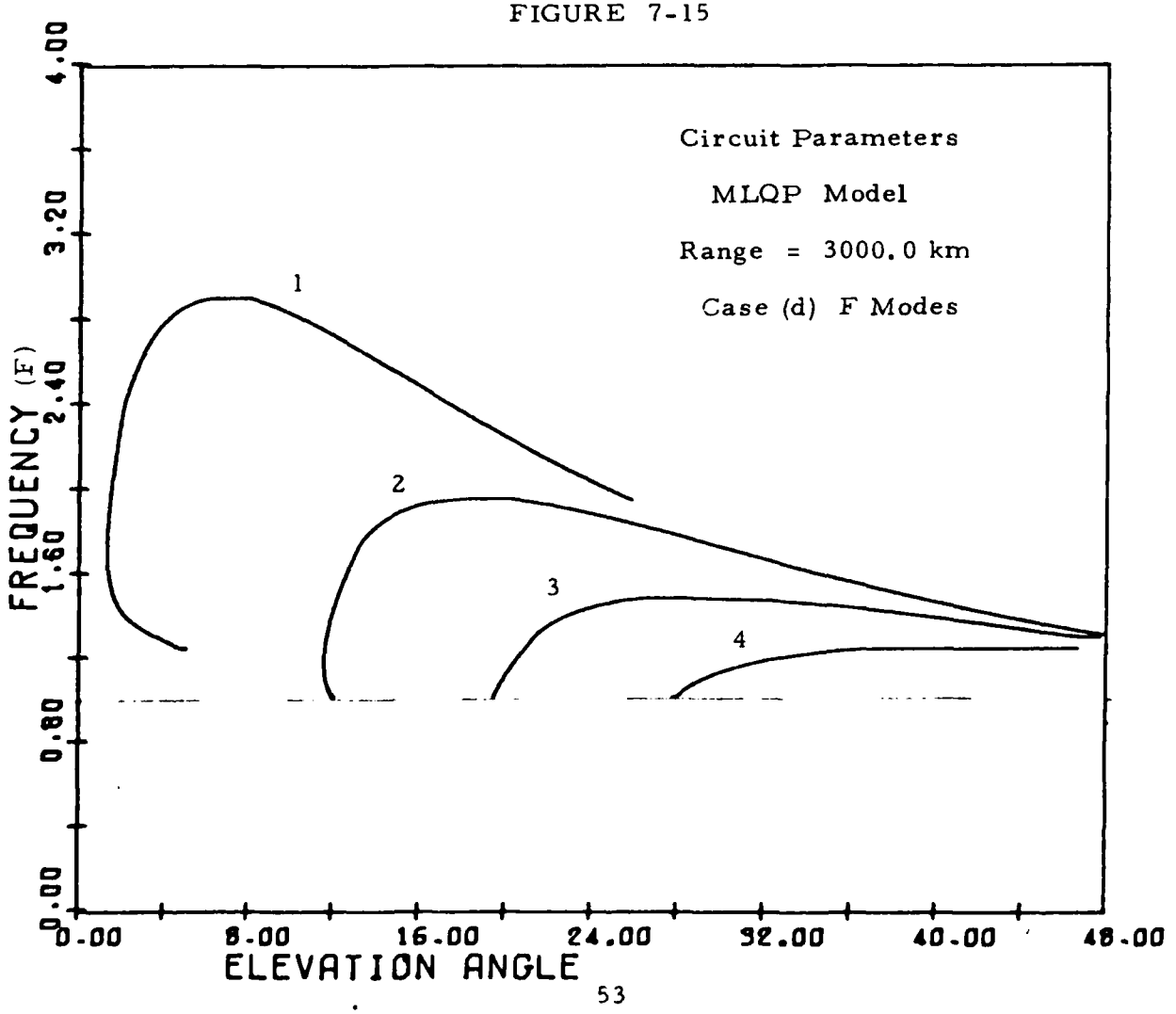
Circuit Parameters
MLQP Model
Range = 3000.0 km
Case (d) F Modes
1
2
3
4
FREQUENCY (F)
4.00
3.20
2.40
1.60
0.80
0.00
0.00
8.00
16.00
24.00
32.00
40.00
48.00
ELEVATION ANGLE

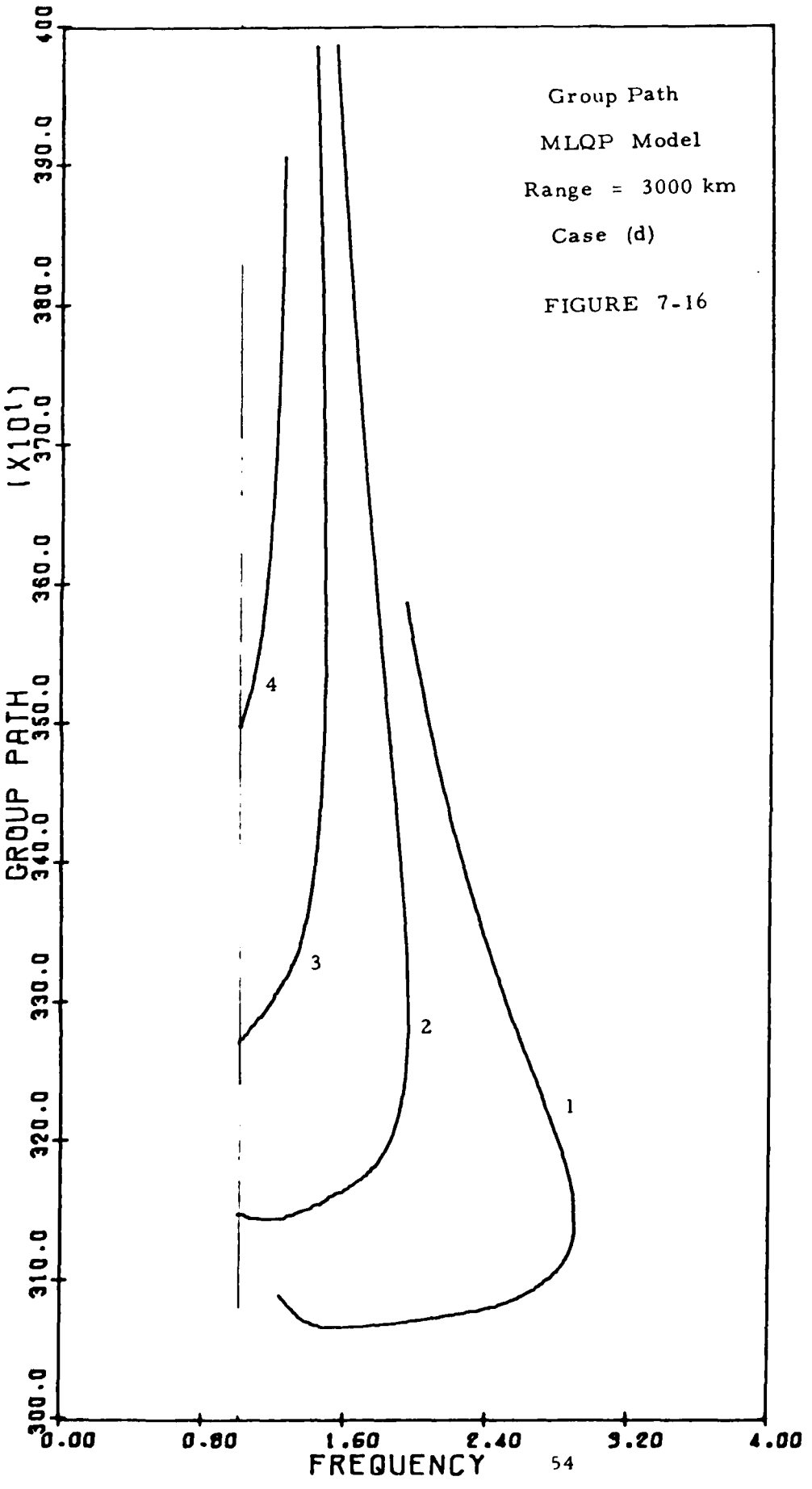
Group Path
MLQP Model
Range = 3000 km
Case (d)
FIGURE 7-16
GROUP PATH (X10¹)
400.0
390.0
380.0
370.0
360.0
350.0
340.0
330.0
320.0
310.0
300.0
0.00
0.80
1.60
2.40
3.20
4.00
FREQUENCY
1
2
3
4

semithickness results in raising the elevation angle necessary to reach the receiver site for a given frequency for the low angle rays. This causes an increase of the group path of ~50 km for the one hop mode and a corresponding increase for each of the multihop modes. Reducing the value of f_oE allows for F mode propagation at smaller elevation angles to the receiver. For these elevation angles the group path is reduced by 50-100 km, independent of the number of ground hops.

An examination of the range curves for models (a) - (d) shows that propagation over distances of 1000-3000 km are characterized by F layer MUF's. By reducing the value of f_oF_2 we can observe the occurence of E layer MUF's. We have used case (e) with a ground range of 2200 km to display these modes. Figure 7-17 shows the circuit parameters required for this range for both the one and two hop E and F modes. Figure 7-18 is the resulting group path for these parameters. The four individual MUF's are shown on Figure 7-17. They are:

One Hop:	F MUF = 17.0MHz.
	E MUF = 18.3
Two Hop:	F MUF = 10.8
	E MUF = 13.0

The method of searching for solutions to the circuit problem is sufficiently sensitive so that all mathematically possible solutions are obtained including those which yield very little energy at the receiver, i.e. when $\frac{\partial R}{\partial \cos 2\beta}$ is very large. Some of the solutions shown on Figure 7-17 are not apparent when the range curve of Figure 7-10 is examined. An example of this is the lowest frequency low angle 1 F mode which almost coincides with a high angle 2 E mode between 14^o and 15^o just under 12MHz.

FIGURE 7-17

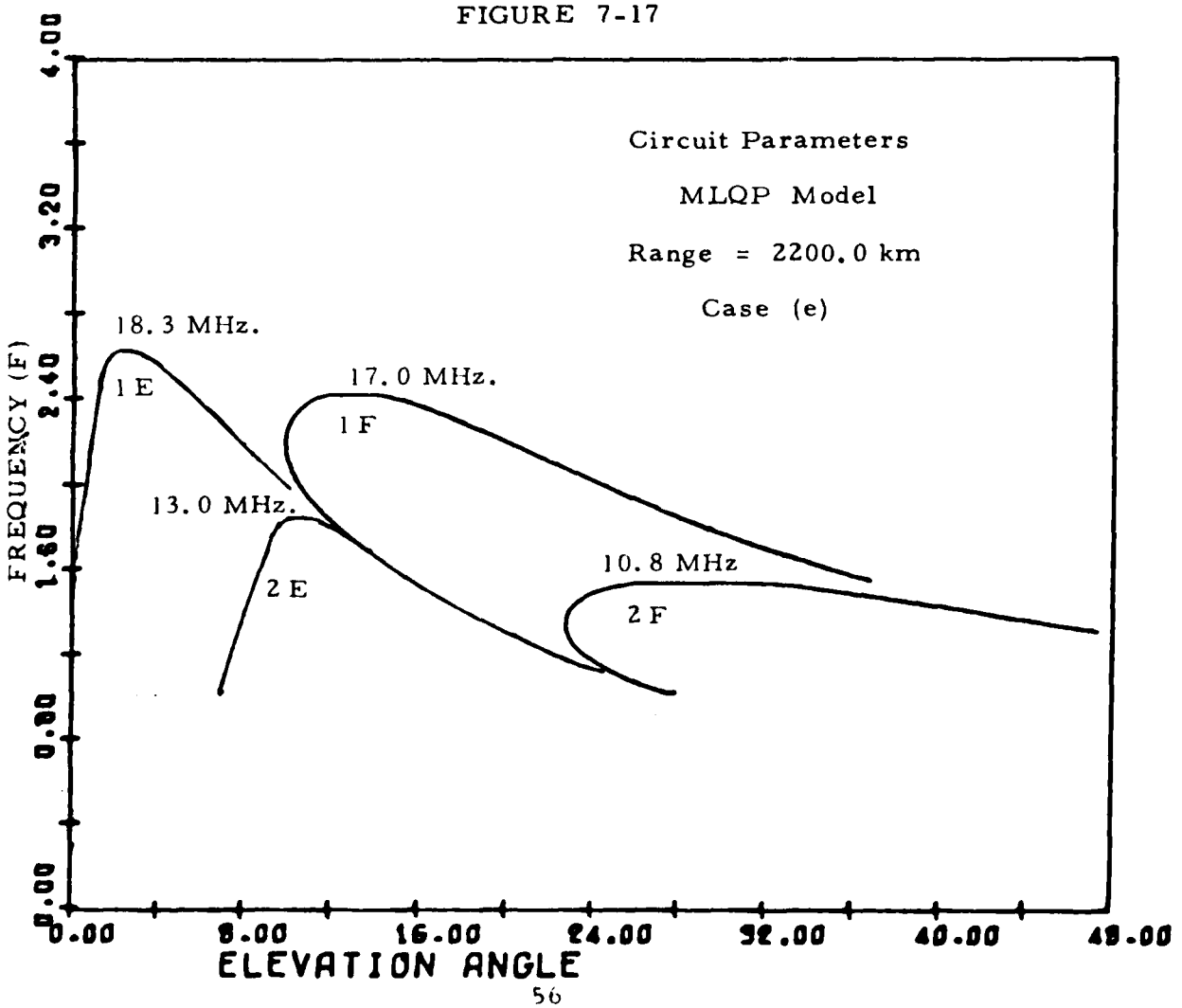
Circuit Parameters
MLQP Model
Range = 2200.0 km
Case (e)
18.3 MHz.
1 E
17.0 MHz.
1 F
13.0 MHz.
2 E
10.8 MHz
2 F
FREQUENCY (F)
4.00
3.20
2.40
1.60
0.80
0.00
0.00
8.00
16.00
24.00
32.00
40.00
48.00
ELEVATION ANGLE

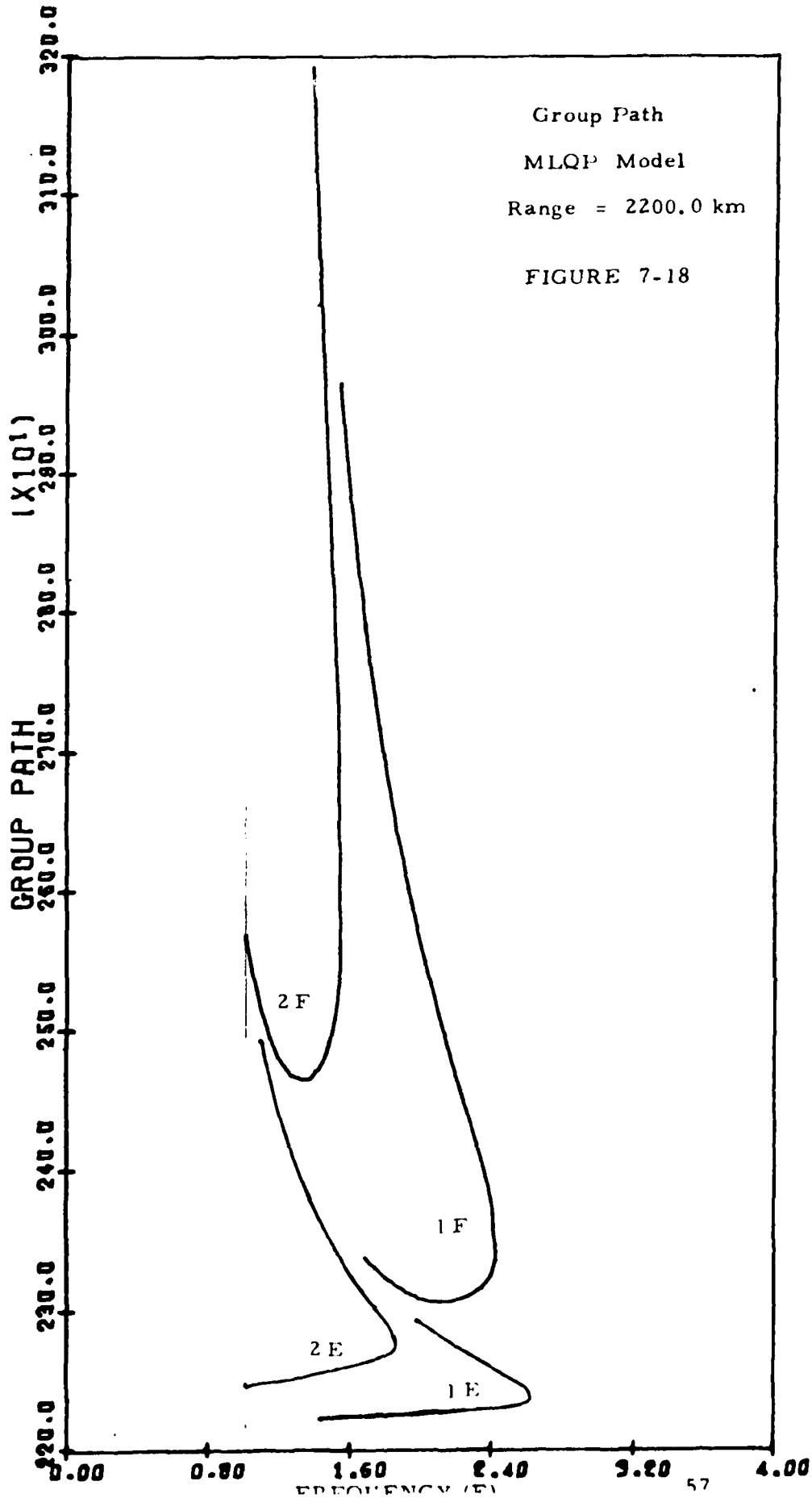
Group Path
MLQP Model
Range = 2200.0 km
FIGURE 7-18
GROUP PATH (X10¹)
320.0
310.0
300.0
290.0
280.0
270.0
260.0
250.0
240.0
230.0
220.0
0.00
0.80
1.60
2.40
3.20
4.00
2 F
1 F
2 E
1 E

The MLQP model has been used to simulate a discrete oblique ionogram for very long ranges in conjunction with a study of high frequency ducted ionospheric modes. Ray tracing programs with electron density models that include horizontal gradients have been used to determine ionospheric conditions that are favorable for ducted propagation. The MLQP model has been used to study the effect of multihop ground modes on the discrete oblique ionogram. Figure 7-19 shows the circuit parameters for F mode multihop propagation over a ground range of 14,000 km. Figure 7-20 is a plot of the group path resulting from these parameters. The calculations were performed using the layer parameters of model (a).

FIGURE 7-19

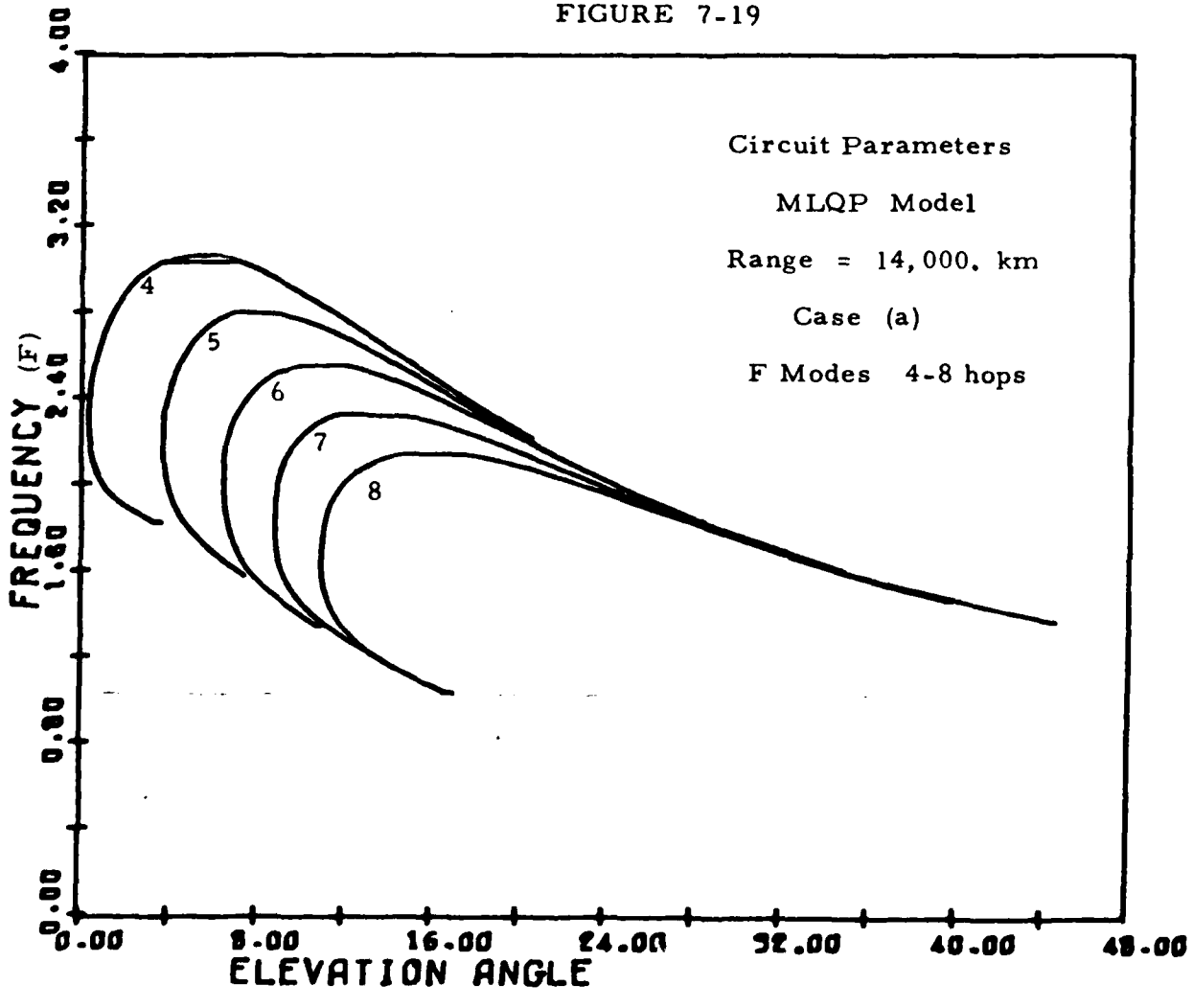
Circuit Parameters
MLQP Model
Range = 14,000. km
Case (a)
F Modes 4-8 hops
4
5
6
7
8
FREQUENCY (F)
4.00
3.20
2.40
1.60
0.80
0.00
0.00
8.00
16.00
24.00
32.00
40.00
48.00
ELEVATION ANGLE

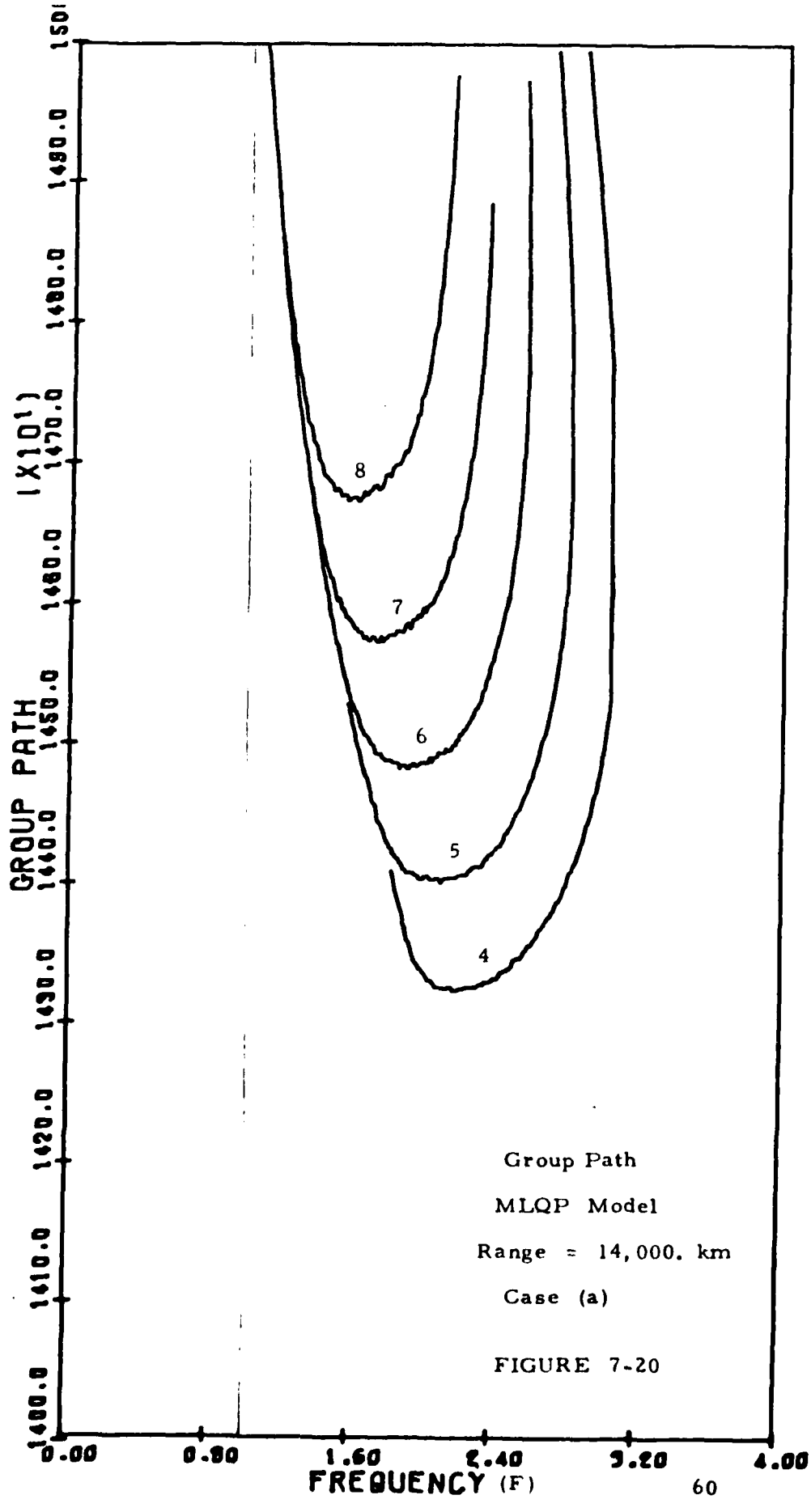

Group Path

MLQP Model

Range = 14,000. km

Case (a)

FIGURE 7-20

8. SIMULATION OF VERTICAL AND OBLIQUE IONOGRAMS

Penultimately the objective of creating ionospheric electron density models and rapid ray calcuation procedures is to provide accurate simulation of RF propagation characteristics in the ionosphere prevailing at the time and place of the simulation. If this accuracy objective is met, the model may then be employed as a reliable tool to estimate system performace characteristics, and target range. This section describes how the electron density model may be finely adjusted based upon the gross and detailed features of vertical and oblique ionograms.

The gross features of the vertical ionogram are used to correct the ionospheric parameters f_oE, f_oF_2, $h'F_2$, $M(3000)F_2$ from which a profile is constructed. The vertical ionogram, virtual height (group path) versus frequency, is then generated.

Five simulations of the vertical ionogram are shown in Figure 8-1. In all of these simulations the primary ionospheric parameters are as follows:

$f_oE = 3.8$Mhz $\quad f_oF_2 = 13.6$Mhz

$h_mE = 110.0$km $\quad h_mF_2 = 333.0$km

$y_mE = 20.0$km $\quad y_mF_2 = 106.4$km

The differences lie in the intermediate layer model between the E and F layer. No ionization produces ionogram A. Ionogram B results from a constant electron density equal to that at the E layer height up to the intersection with the F layer. Ionogram C is produced from an inverted QP layer joining the E layer smoothly at h_mE to the intersection

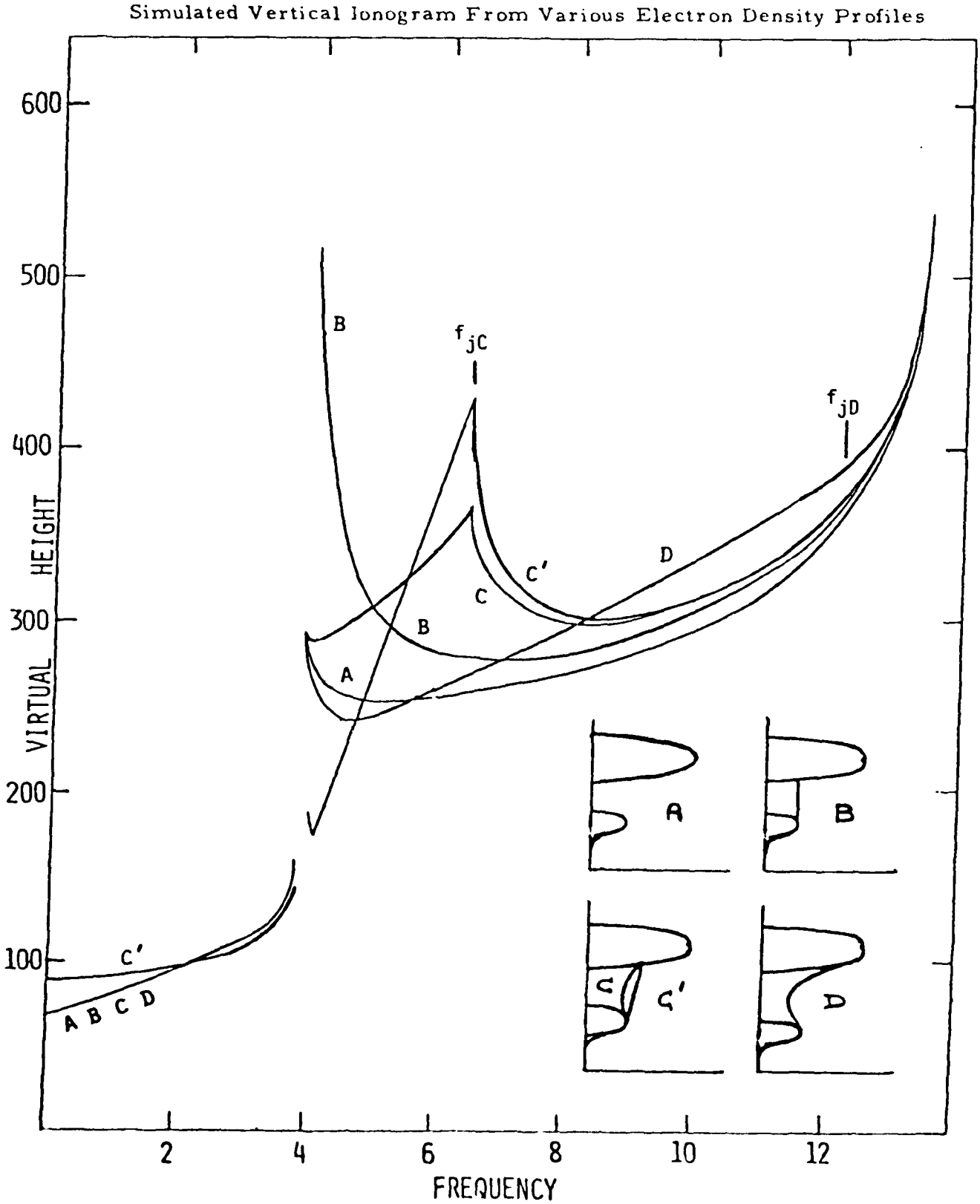
Simulated Vertical Ionogram From Various Electron Density Profiles
600
500
400
300
200
100
VIRTUAL HEIGHT
B
f_{jC}
f_{jD}
C'
D
C
B
A
C'
A B C D
A
B
C
C'
D
2
4
6
8
10
12
FREQUENCY

FIGURE 8-1

on the F layer where the plasma frequency equals 1.7 $f_o E$, while C' results from the modified Bradley-Dudeney profile. The piecewise smooth QP layer with the scale independant criterior results in ionogram D. The fitting points and plasma frequencies for these models are listed in Table 8.1.

It is clear from inspection of Figure 8-1 that the choice of electron density model between the E and F layer has a considerable effect upon the detailed structure of the vertical ionogram.

The piecewise smooth QP profile using the scale independant criterior (ionogram D) tends to flatten out the belly from the QP layer model (ionogram A), while a shelf tends to strongly lift the curve just above $f_o E$ (ionogram B). Electron density Model C is close to the Bradley-Dudeney profile except that the intermediate layer is tangent to the E layer at $h_m E$; ionogram C tends to rise more or less linearly just above $f_o E$, characteristic of the inverted QP behavior to a cusp singularity at f_j. Above f_j the ionogram displays the concavity characteristic of the QP layer. Note, however, that the cusp at f_j is much less severe than that produced by the Bradley-Dudeney profile.

The scale independent criterion for the construction of the intermediate layer generates a fitting point high up on the F layer, while the ionogram to be modeled displays a pronounced belly similar to ionogram A. Adjustment of the F layer height and semi thickness does not overcome this difficulty, which reappears in the context of simulating the oblique ionogram, discussed below.

Clearly, the question of the intermediate ionization model requires more study using a larger sample of ionograms, and the systematics of selecting the best intermediate layer model developed.

TABLE 8-1

Parameters for Intermediate Layer Models

Model Layer	h_I	h_L	h_J	f_I	f_L	f_J
A	130	130	227	0	0	0
B	110	110	231	3.80	3.80	3.80
C	110	110	239	3.80	3.80	6.46
C'	110	-	239	3.80	-	6.46
D	112	127	282	3.78	3.60	11.98

The main feature of the oblique backscatter ionogram to simulate is the leading edge. The basic problem is, for a given ionosphere and at a given frequency, find that ray (selected by elevation angle) that corresponds to the minimum group path length (MGP), or, equivalently, locate a zero in the derivative of the group path function of take off elevation (or its cosine). We shall discuss the MGP solution for F layer reflections; there would be no substantial difference, however, should one desire the E layer MGP solutions.

A minimum in the group path length occurs because of the maximum in the electron density at the F layer height. As one increases the elevation angle from low angles the group path decreases, and to a first approximation the situation is similar to single reflection from a fixed plane mirror. This simple model is inadequate in two respects. Firstly, the actual penetration into the ionosphere increases with elevation, and secondly, the time delays increase. Thus, we need to float the mirror upwards as we increase the elevation to keep pace with the virtual height, tending to increase the group path length. As the virtual frequency

approaches the critical frequency of the layer, the group path length increases without bounds; this increase, then, will eventually dominate the previous decrease and thus a minimum in the group path length will occur. Rays at elevations less than that corresponding to the minimum are the "low angle" rays, for which a geometric path loss model applies quite well. The group path-elevation curve increases quite sharply above that angle, resulting in rapid decrease in energy density and additional losses must be allocated. Note that, at the minimum, focusing occurs resulting in signal enhancement.

During traversal of a ray through an inverted QP layer, the group path decreases with increasing elevation angle, it is only after entering a QP layer when the group path increases. This establishes a search window for the minimum group path solution between penetration into the F_2 layer and penetration through the F_2 layer.

Penetration into the F_2 layer occurs when the function $Z(r_j)$ given by equation 3.4 vanishes, where r_j is the point at which the intermediate inverted QP layer meets the QP F_2 layer, or at the angle β_{oj} given by

$$\cos^2\beta_{oj} = (r_j/r_o)^2 \quad (1 - kN(r_j)/f^2)$$

Penetration through the F_2 layer occurs when the discriminant of the function $Z(r)$ given in equation 3.4 vanishes, or at the angle β_{oF} given by

$$\cos^2\beta_{oF} = (r_m/r_o)^2 \, X_G \, (1 - X_C)/(1 - X_C + X_G)$$

where the other terms are as defined following equation 3.4.

The convenient independant variable to employ in lieu of the takeoff elevation angle β_o is the square of its cosine, $x = \cos^2\beta_o$. The solution

for the minimum group path at x_m will be found in the domain given by

$$x_j \geq x_m \geq x_F$$

This interval is divided, by convenience, into eight equal interval segments of width $\Delta = (x_F - x_j)/8$. To start the search process, three rays are calculated yielding group paths $P_k = P(x_k)$ where $x_k = x_j + k\Delta$, $k = 1, 2, 3$.

Numerical estimates of the derivatives of $P(x)$ are calculated as

$$P'_A = P'(x_A) = (P_2 - P_1)/(x_2 - x_1)$$
$$P'_B = P'(x_B) = (P_3 - P_2)/(x_3 - x_2)$$

where $x_A = (x_1 + x_2)/2$

and $x_B = (x_2 + x_3)/2$

The first and second derivatives of the function $P(x)$ are estimated by

$$P'_o = P'(x_o) = (P'_A + P'_B)/2$$
$$P''_o = P''(x_o) = (P'_A - P'_B)/(x_A - x_B)$$

where $x_o = (x_A + x_B)/2$.

In the neighborhood of x_o, the group path function $P(x)$ may be approximated as

$$P(x) = P(x_o) + P'(x_o)(x - x_o) + 1/2\, P''(x_o)(x - x_o)^2$$

and its derivative by

$$P'(x) = P'(x_o) + P''(x_o)(x - x_o)$$

At the minimum of $P(x)$ its first derivative must vanish, thus a correction to x is generated as

$$\delta x = - P'_o/P''_o$$

The points x_2 and x_3 are demoted to the roles of points x_1 and x_2 respectively, while a new value of x_3 is given by

$$x_3 = x_o + \delta x.$$

A new ray is calculated yielding $P_3 = P(x_3)$.

The iteration continues until P_3 is within 0.5 kilometers of the most recently calculated minimum value, except that no more than eight rays are calculated. Escape from the iterative process usually occurs after the minimum of four rays; a single correction is generally sufficient. Rarely is it necessary to calculate six or more rays.

Having located the minimum group path solution at the given frequency for the specified model ionosphere, the model ionosphere may be updated to take into account horizontal variations of the ionospheric characteristics, both by creating a new synthetic ionosphere and by calculating layer by layer changes in the elevation angle due to the horizontal gradients. With this new ionosphere, the minimum group path algorithm may be reentered to improve the soltuion. This process is reiterated until the desired convergence criterior is attained.

This iterative ionospheric parameter updating/direction cosine correction process could be accomplished within the iterative search for minimum group path ray by ray or even layer by layer within a ray calculation. This may speed up the iteration process; on the other hand, such a double correction may lead to instabilities or oscillations, and may actually slow up the process. Furthermore, the parameter correction scheme to fit a given oblique ionogram depends upon the result of the simulation of the leading edge point, and the double iteration is required in any case.

The technique described in Section 6 for the development of a f_oF_2 versus range function was applied to the simulation of the leading edge of an actual oblique ionogram. The function so developed is shown in Figure 8.2 together with the ITS model for f_oF_2 (corrected to the vertical ionogram parameters). Also the linear fit f_oF_2 is displayed.

The forced fit model exhibits oscillations. This behavior may in fact be real, due perhaps to an ionospheric disturbance with a 500 kilometer wavelength. On the otherhand, the oscillations may be due to computational prejudices such as arbitrarily selecting f_oF_2 as the only parameter allowed to deviate from the ITS model. Clearly, h_mF_2 and y_mF_2 have significant influence in determining the shape of the leading edge.

The oblique backscatter ionogram was simulated using three models for f_oF_2: (1) the ITS climatological model, (2) the linear fit model based upon the forced fit process, and (3) the overhead value of f_oF_2 at the transmit site. The results of these simulations are shown in Figure 8.3, and residuals are given in Table 8.2. Clearly, the linear fit model is significantly better than the ITS model. The transmit site value produces results nearly as good as the linear fit model; however, this may only be fortuitous.

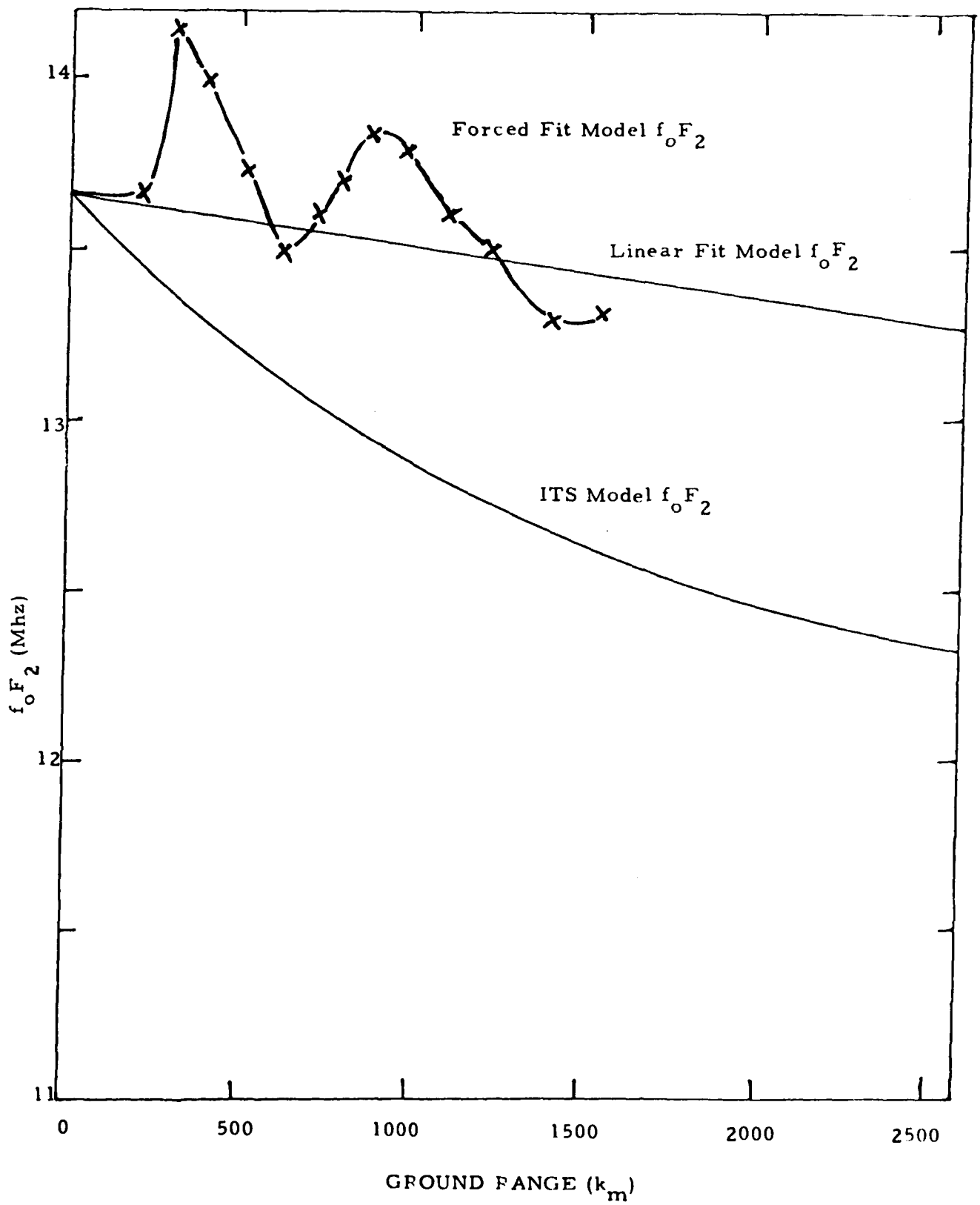
Forced Fit Model f_oF_2
Linear Fit Model f_oF_2
ITS Model f_oF_2
14
13
12
11
f_oF_2 (Mhz)
0
500
1000
1500
2000
2500
GROUND RANGE (k_m)

FIGURE 8-2

TABLE 8-2

Residuals of Oblique Ionogram Simulation
With Various f_oF_2 Models

Frequency MH_z	Overhead Value	Residuals From Linear Fit Model	ITS Model
14	+ 7.8 km	+ 3.0 km	+ 15.8 km
16	+47.6	+42.3	+ 65.3
18	+42.0	+36.2	+ 71.2
20	+21.8	+15.5	+ 65.2
22	- 1.7	- 8.6	+ 58.0
24	+12.6	+ 4.4	+ 87.8
26	+36.6	+26.6	+131.3
28	+72.4	+60.2	+192.1
30	+72.8	+58.0	+226.0
32	+41.8	+23.8	+241.7
34	+35.2	+13.2	+289.1
36	-38.1	-68.2	+295.2
38	-12.7	-55.9	+434.3

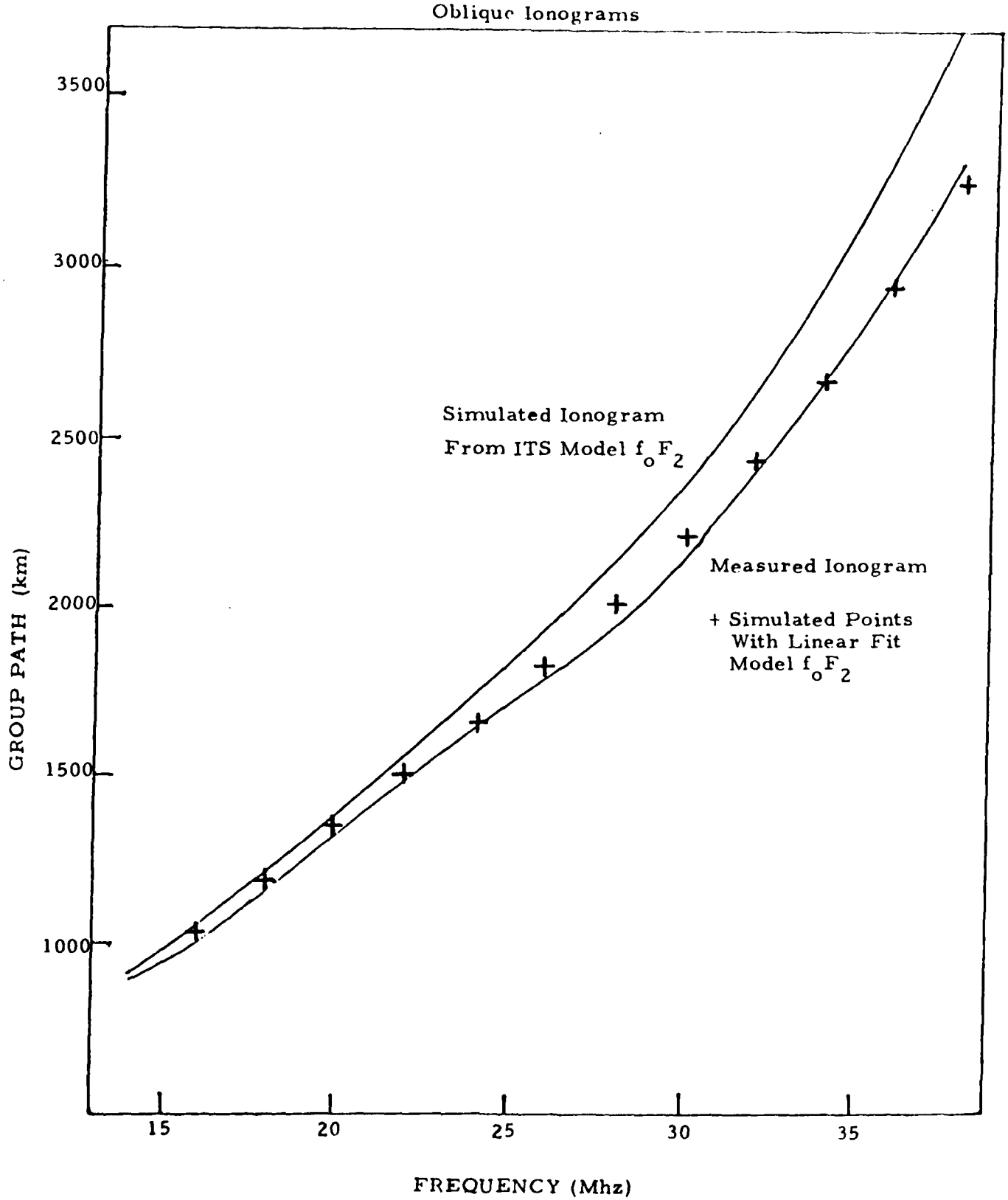
Oblique Ionograms
3500
3000
2500
2000
1500
1000
GROUP PATH (km)
Simulated Ionogram
From ITS Model f_oF_2
Measured Ionogram
+ Simulated Points
With Linear Fit
Model f_oF_2
15
20
25
30
35
FREQUENCY (Mhz)

FIGURE 8-3

MISSION
of
Rome Air Development Center

RADC plans and executes research, development, test and selected acquisition programs in support of Command, Control Communications and Intelligence (C^3I) activities. Technical and engineering support within areas of technical competence is provided to ESD Program Offices (POs) and other ESD elements. The principal technical mission areas are communications, electromagnetic guidance and control, surveillance of ground and aerospace objects, intelligence data collection and handling, information system technology, ionospheric propagation, solid state sciences, microwave physics and electronic reliability, maintainability and compatibility.

Printed by
United States Air Force
Hanscom AFB, Mass. 01731


DATE
ILMED
-8